Quaternary morphotectonic mapping of the Wadi Araba and implications for the tectonic activity of the southern Dead Sea fault

Maryline Le Béon,[1,2,3] Yann Klinger,[1] Anne-Sophie Mériaux,[4] Mahmoud Al-Qaryouti,[5] Robert C. Finkel,[6,7] Omar Mayyas,[5] and Paul Tapponnier[1,8]

[1]   The Dead Sea strike-slip fault accommodates the northward motion of Arabia relative to Sinai at a rate of ∼5 mm/yr. The southern segment of the fault, the Wadi Araba fault, runs along a valley blanketed in Quaternary sediments. We first focused on understanding the relative and absolute timing of emplacement of the alluvial surfaces. We then determined the probable source of the sediments before assessing their lateral offset to constrain the late Pleistocene fault slip rate. Seven successive morphostratigraphic levels were identified. At two sites, we recognized an alluvial sequence of five to seven successive levels with ages getting younger northward, a pattern consistent with the western block moving southward relative to two fixed feeding channels located to the east. Surface samples were collected for ^{10}Be cosmogenic radionuclide dating. Fans F3 and F5 were found to be synchronous from site to site, at 102 ± 26 ka and 324 ± 22 ka, respectively, while F4 could be dated at 163 ± 19 ka at one site only. These are minimum ages, assuming no erosion of the alluvial surfaces. At least two of these periods are correlated with wet periods that are regionally well documented. Further analyses of tectonic offsets are affected in most cases by large uncertainties due to the configuration of the sites. They indicate maximum offsets of ∼5.5 km for the oldest, possibly ∼1 Ma old, surfaces. They lead to bracketing of the fault slip rate between 5 and 12 mm/yr, with preferred values of 5–7 mm/yr, for the last 300 ka.

Citation: Le Béon, M., Y. Klinger, A.-S. Mériaux, M. Al-Qaryouti, R. C. Finkel, O. Mayyas, and P. Tapponnier (2012), Quaternary morphotectonic mapping of the Wadi Araba and implications for the tectonic activity of the southern Dead Sea fault, *Tectonics*, *31*, TC5003, doi:10.1029/2012TC003112.

1.   Introduction

[2]   The Dead Sea fault is the 1000 km long left-lateral strike-slip fault that accommodates the northward motion of the Arabia plate relative to the Sinai subplate (Figure 1a). Numerous studies aimed to determine the slip rate of this fault based on geological observations over the last ∼20 Ma [*Dubertret*, 1932; *Quennell*, 1958, 1959; *Freund et al.*, 1968, 1970; *Hatcher et al.*, 1981; *Courtillot et al.*, 1987; *Garfunkel and Horowitz*, 1966; *Garfunkel*, 1981; *Garfunkel and Ben-Avraham*, 2001], offset markers of Quaternary age [*Klinger et al.*, 2000a; *Niemi et al.*, 2001; *Daëron et al.*, 2004; *Marco et al.*, 2005; *Ferry et al.*, 2007, 2011; *Makovsky et al.*, 2008; *Le Béon et al.*, 2010], and GPS measurements [*Wdowinski et al.*, 2004; *Reilinger et al.*, 2006; *Le Béon et al.*, 2008, *Alchalbi et al.*, 2010]. These different studies converge to a mean value of 4–6 mm/yr between present and 20 Ma ago. Some, however, suggest that the slip rate could have been as high as ∼10 mm/yr during the late Pleistocene [*Klinger et al.*, 2000a; *Le Béon et al.*, 2010].

[3]   South of the Dead Sea basin, the Dead Sea fault runs near the axis of a broad valley, the Wadi Araba valley (the term "wadi" meaning "river"). This valley, which is 160 km long, is bordered by the steep rims of the Jordanian Plateau to the east and of the Negev Plateau to the west (Figure 1b). The depression exhibits highly preserved landscape thanks to local arid climatic conditions. The valley floor is blanketed in Quaternary sediments of various types (Figure 2),

[1]Institut de Physique du Globe de Paris, Sorbonne Paris Cité, Université Paris Diderot, UMR 7154, CNRS, Paris, France.
[2]Department of Geosciences, National Taiwan University, Taipei, Taiwan.
[3]Now at Institute of Earth Sciences, Academia Sinica, Taipei, Taiwan.
[4]School of Geography, Politics and Sociology, Newcastle University, Newcastle upon Tyne, UK.
[5]Seismology Division, Natural Resources Authority, Amman, Jordan.
[6]Earth and Planetary Science Department, University of California, Berkeley, California, USA.
[7]Center for Accelerator Mass Spectrometry, Lawrence Livermore National Laboratory, Livermore, California, USA.
[8]Earth Observatory of Singapore, Nanyang Technological University, Singapore.

Corresponding author: M. Le Béon, Institut de Physique du Globe de Paris, Sorbonne Paris Cité, Université Paris Diderot, UMR 7154, CNRS, 1 rue Jussieu, F-75005 Paris, France. (lebeon@ipgp.fr)
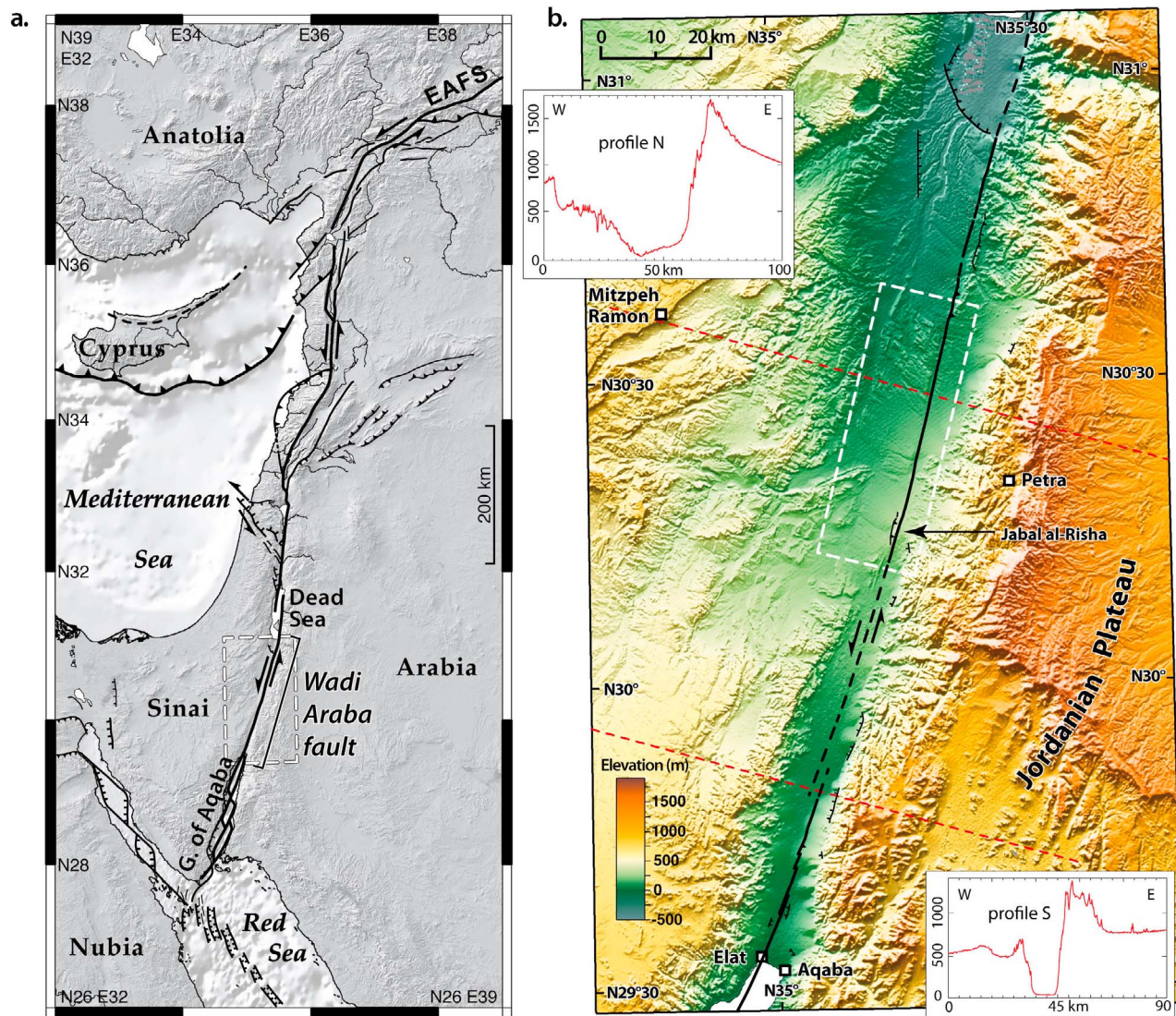
Figure 1. (a) Regional tectonic setting of this study. Tectonic map modified from *Daëron et al.* [2004] and *Elias et al.* [2007]. EAFS, East Anatolian fault system. Box indicates location of Figure 1b. (b) SRTM3 topography and active faults of the Wadi Araba. White rectangle indicates the large alluvial fans our study focuses on. Red lines show location of inset topographic profiles.

distinguishable on satellite images: aeolian sand dunes, playa deposits, lacustrine marls, and alluvial deposits [e.g., *Bender et al.*, 1968; *Garfunkel et al.*, 1981; *Sneh et al.*, 1998a, 1998b; *Klinger et al.*, 2003]. In the central part of the valley (Figures 1b and 2), 10 km scale abandoned alluvial surfaces are easily noticeable, due to their darker color and their sharp eastern edge, controlled by the active trace of the Wadi Araba strike-slip fault (WAF) [*Garfunkel et al.*, 1981]. Published geological maps do not converge toward a consistent chronology, either relative or absolute, for the emplacement of these alluviums. Periods of deposition vary from Miocene to Pleistocene ages [*Bartov*, 1994; *Sneh et al.*, 1998a, 1998b, 2000], or from early Pleistocene to Holocene ages [e.g., *Bender et al.*, 1968; *Bender*, 1974; *Ibrahim*, 1990; *Rabb'a*, 1991, 1994; *Tarawneh*, 1991; *Barjous*, 1995, 2003].

[4] In order to determine the origin and ages of these alluvial deposits, we conducted a detailed morphotectonic analysis of the Wadi Araba that was complemented by [10]Be

cosmogenic radionuclide (CRN) dating of alluvial surfaces and analysis of the Wadi Araba tributary catchment areas (the main ephemeral river that occupies the northern half of the valley). In a first step, the units are described at the scale of the valley. Then, we focus on three sites that we have investigated in detail: Risha and al-Dhawi, Mazla, and Fuhud/Masqara (Figure 3). For these sites we describe the tectonic geomorphology and the [10]Be CRN model ages. Finally, we discuss the synchronism of alluvial deposition in the valley in respect to paleoclimates and examine evidence for left-lateral displacements that we attempt to quantify before estimating the long-term slip rate along the WAF.

2. Morphotectonic Map of the Wadi Araba

2.1. Data and Morphologic Criteria

[5] Relative ages of alluvial surfaces can be distinguished as a function of surface height above active streams, degree
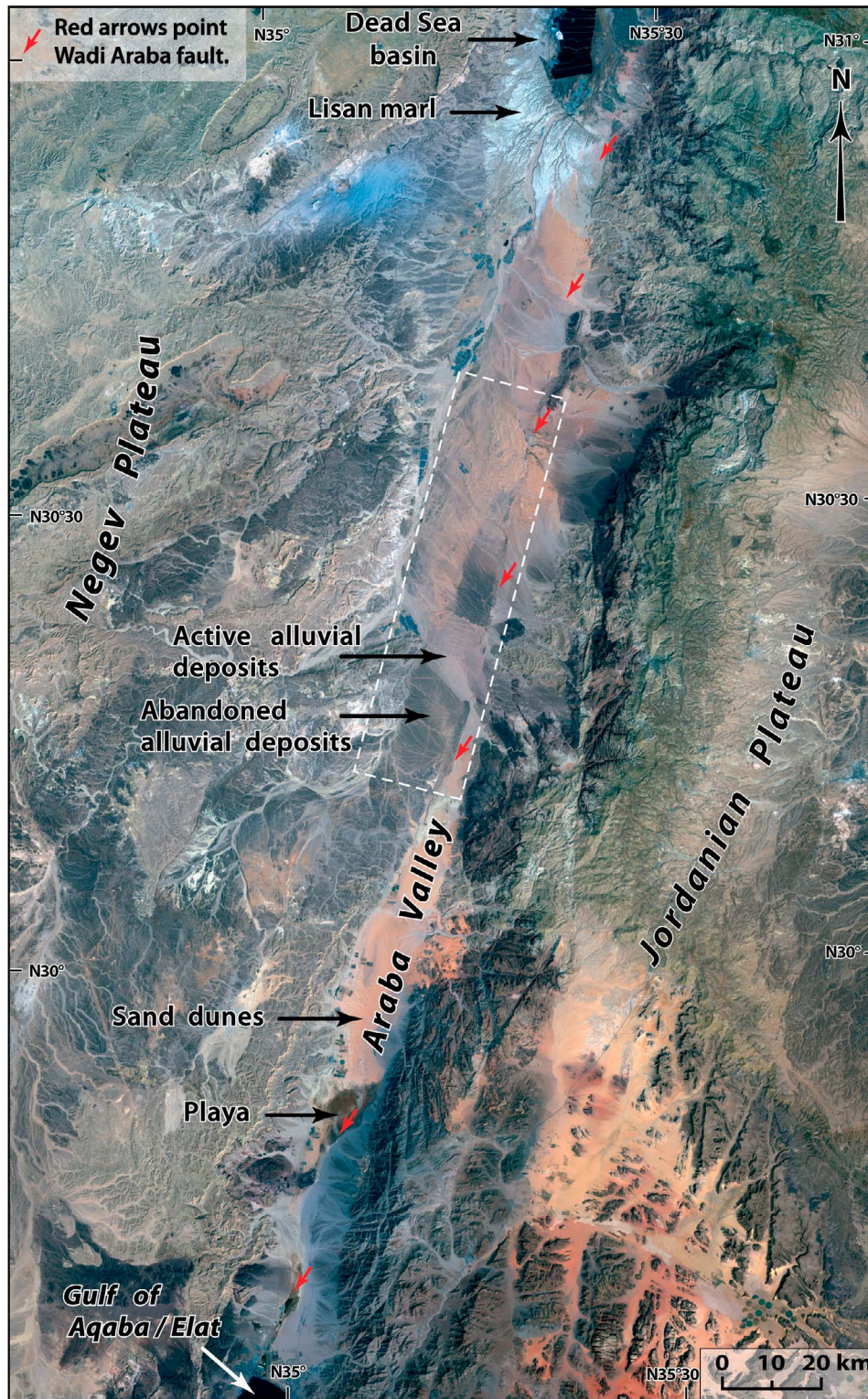
Figure 2. Landsat7 satellite view of the Wadi Araba, illustrating the different types of Quaternary sediments that cover the valley floor. White box indicates the large alluvial surfaces which we focus on in this study.

of incision by surficial rills and regressive gullies, surface darkness and geometric relationship between the deposits [e.g., *Klinger et al.*, 2003; *Le Béon et al.*, 2010]. For example, darker surfaces, related to desert varnish and desert pavement, typical in arid areas, indicate older surfaces [*Bull*, 1991; *Quade*, 2001]. Observations have been derived from satellite imagery (Landsat7, SPOT5 (pixel ~2.5 m), high-resolution Google Earth database), aerial photographs,
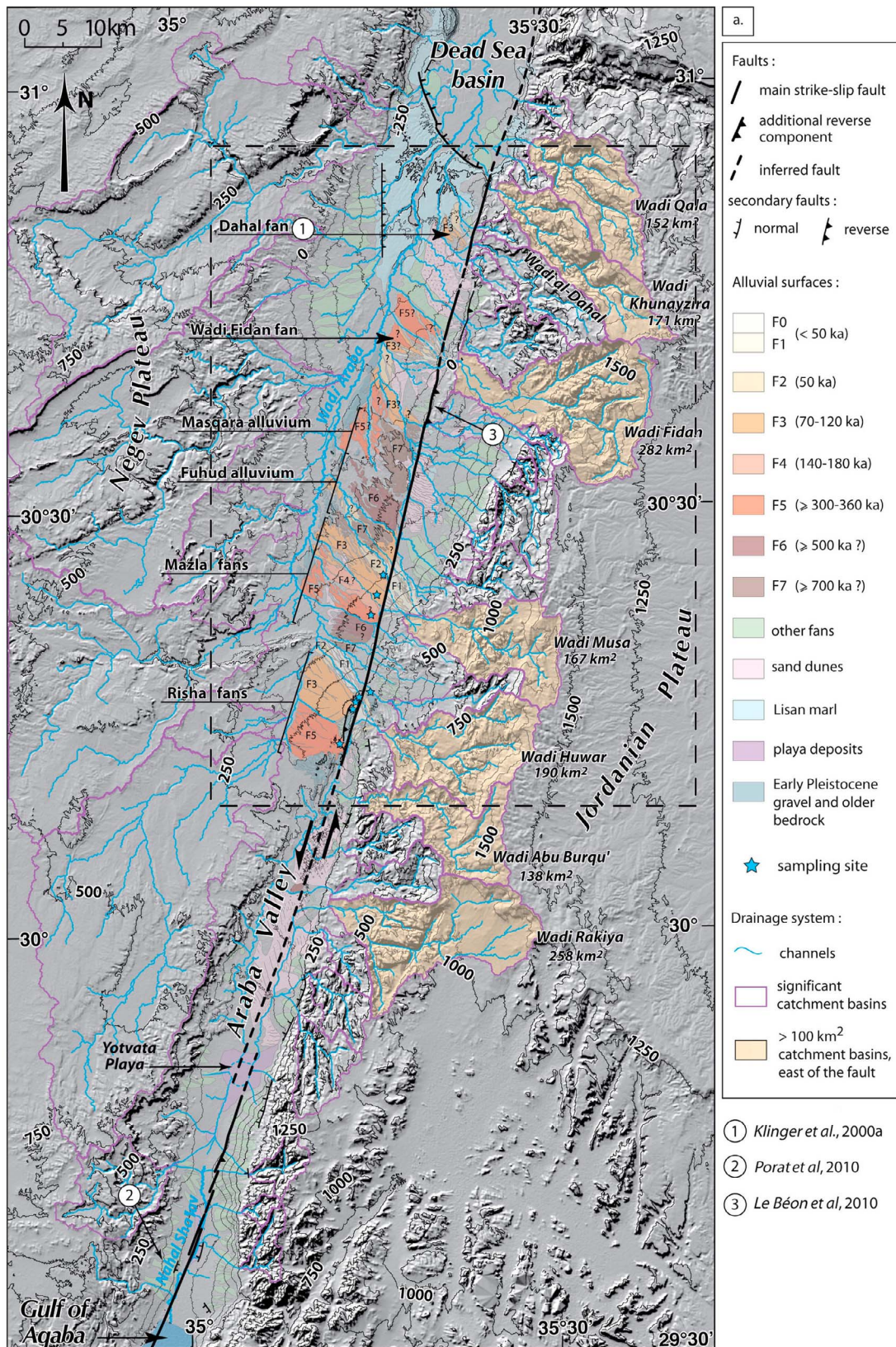
Figure 3. (a) Morphotectonic map and drainage network of the Wadi Araba. Box shows location of Figure 3b. (b) Morphotectonic map of the northern Wadi Araba. See legend on Figure 3a. Boxes show location of detailed morphotectonic maps of the large abandoned alluvial fans. Question marks indicate uncertain correlations of alluvial surfaces far from any absolute age constraints. A georeferenced version of the morphotectonic map, with the level of details presented in Figures 4 to 6, is available in auxiliary material Data Set S1.
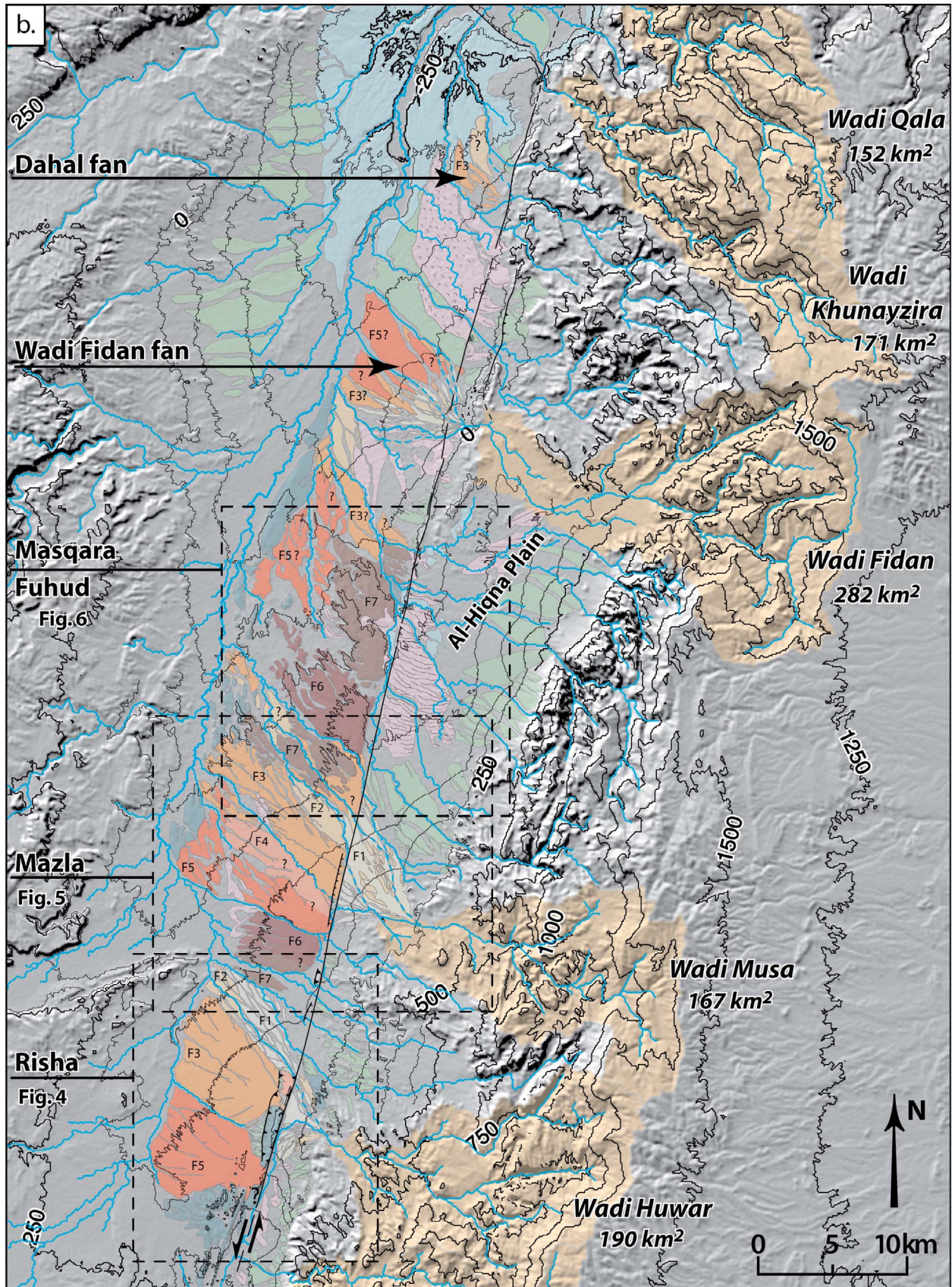
Figure 3. (continued)

1/50,000 topographic maps, SRTM3 and ASTER (pixel ~30 m) topography and field observations at key locations. Information on the geological setting was derived from 1/250,000 and 1/50,000 geological maps referenced hereafter.

2.2. The Active Trace of the Wadi Araba Fault

[6] The active fault cuts the Quaternary deposits along a single strand striking ~N15°E (Figures 1b and 3). Numerous coseismic [*Klinger et al.*, 2000b] and cumulative offsets [e.g., *Garfunkel et al.*, 1981; *Amit et al.*, 1996; *Klinger et al.*, 2000a; *Niemi et al.*, 2001; *Le Béon et al.*, 2010] of geomorphic features, such as channels and alluvial surfaces, can be observed. Push-up structures and pull-apart basins occupied by dry playas or filled with alluvial sediments are found as well. Between Risha and the Yotvata Playa (Figure 3a), sand dunes hamper an accurate determination of the fault location. However, assuming that the fault azimuth is constant along this section (dashed line in Figures 1b and 3a), we suggest that the Yotvata Playa actually corresponds to a left-stepping extensional jog of the fault. Further south, the fault is clearly visible until the town of Elat where it enters the Gulf of Aqaba [*Makovsky et al.*, 2008]. Minor normal faults affecting the Quaternary alluvium abutting onto the edge of the valley are also observed in a few places, mostly on the eastern valley edge.

2.3. The Quaternary Sedimentary Cover

[7] The morphotectonic map is presented on Figure 3. The color code from brown (older) to light yellow (younger) defines a relative chronology for the emplacement of the middle to late Pleistocene alluvial deposits at the scale of the Wadi Araba. These deposits have been subdivided into seven morphostratigraphic levels, F7 to F1 (F1 being the youngest); F0 refers to active washes. Detailed mapping based on the combination of geomorphic analyses at the sites of Risha and al-Dhawi, Mazla, and Fuhud/Masqara, which are discussed in details in section 4, is used as reference to further expand the map to the entire Wadi Araba surfaces. The surface correlation from site to site was established from [10]Be CRN model ages (section 5) for surfaces F5 and F3. We also accounted for previously published geomorphic mapping and [10]Be age data for the Wadi al-Dahal alluvial fan, located in the northern Wadi Araba (Figures 1b and 3) [*Klinger et al.*, 2000a, 2003]. For the other surfaces, the proposed relative chronology is based on geomorphic criteria and on the assumption that climatic events are synchronous at the scale of the studied area (section 6.1) [e.g., *Bull*, 1991]. Uncertain correlations of alluvial fans far from any published data or from the sites of this study are indicated by question marks on the map.

[8] The sedimentary cover evolves from south to north, in relation with the topography of the valley rims (Figures 2 and 3). In the south, alluvial fans of similar size (1 to 3 km in diameter) were emplaced on both sides of the valley and coalesce in the center. This pattern probably reflects the pseudosymmetry of the valley rims (see topographic profile on Figure 1b), roamed by steep and short catchments on either side. A few playas occupy the valley bottom. A vast sand dunes field lies from the Yotvata playa to the Jabal al-Risha.

[9] North of the Jabal al-Risha, along the central section of the Wadi Araba valley, the sedimentary cover is dominated by active and abandoned large alluvial surfaces, sprinkled with sand dunes in some places. Differences in height, darkness, and degree of incision of the alluvial surfaces suggest deposits of varying ages. From the Jabal al-Risha to the Wadi Fidan fan, large alluvial surfaces, locally crosscut by the fault, gently dip to the west and fill the valley over its entire width, pushing westward the Wadi Araba thalweg. The alluvial fans located along this section of the Wadi Araba are generally much larger than further south, due to larger catchment areas. The asymmetry of the alluvial fill probably reflects the asymmetry of the valley rims (Figure 1b). To the east, the catchments are large and steep, with rivers constrained to narrow canyons. To the west, instead, the drainages coming down the Negev Plateau have wider riverbeds with gentler slopes and flow toward the NE, following the general direction of the folded structures forming the topography (Figures 2 and 3).

[10] West of the fault, at the sites of Risha, Mazla, and Fuhud/Masqara, 10 km scale alluvial surfaces stand out due to their dark surficial color related to desert varnish, high elevation above the active streams and/or a developed network of surficial rills and regressive gullies. In addition to the sharpness of their eastern edge, bounded by the active trace of the WAF, some of the alluvial surfaces, especially at Risha, are characterized by radial topographic contour lines, concave to the east. This morphology attests that they originate from major catchments coming down the edge of the Jordanian Plateau to the east. Because the large alluvial surfaces of Risha, Mazla, and Fuhud/Masqara lie west of the WAF and originate from the east, they were progressively disconnected from their source. Being shuttled along the fault, they can be used to constrain the fault activity, as outlined in section 4.

[11] North of the Wadi Fidan fan, coalescent alluvial deposits (i.e., bajada) occupy both sides of the valley. The northernmost deposits dip toward the Dead Sea basin and are interfingered with the white Lisan marls that formed when the Lake Lisan, the precursor of the Dead Sea, reached elevations up to 180 to 150 m bsl (below sea level) in the late Pleistocene [e.g., *Kaufman et al.*, 1992; *Bartov et al.*, 2002; *Klinger et al.*, 2003; *Waldmann et al.*, 2007]. The soft marls are deeply incised due to considerable lake level drop since the early Holocene [e.g., *Frumkin*, 1997] and to down drop of the basin north of the Khunayzir (Amatzia) normal fault.

3. The Possible Sources for the Large Alluvial Fans

[12] In order to use the large abandoned alluvial surfaces to quantify geomorphic offsets related to motion of the WAF, one needs first to identify the feeding catchment associated with each fan. The Wadi Araba drainage network was investigated based on satellite topographic data SRTM3 (pixel ~90 m) (http://www2.jpl.nasa.gov/srtm/) processed with the RiverTools software. The catchments and drainage network are shown on Figure 3. Detailed descriptions are given by *Greenbaum et al.* [2006] and *Le Béon* [2008]. Due to arid climate, most drainages are actually occupied by ephemeral rivers or streams.

[13] We need to determine which of the catchments on the eastern valley rim of the Wadi Araba were able to produce alluvial deposits of such size. It has been shown that the

extent of an alluvial fan is proportional to the area of its feeding catchment [e.g., *Bull*, 1962; *Harvey*, 1997; *Rohais*, 2007]. This relation is modulated by a constant that accounts for parameters such as climate, tectonics, and the erodability of the exposed rocks. Since these parameters do not vary significantly along the eastern rim of the northern and central sections of the Wadi Araba, the main criterion we need to take into account is the catchment area.

[14] To calibrate the size of such catchment, we rely on the Wadi al-Dahal alluvial fan located in the northern Wadi Araba (Figure 3). *Klinger et al.* [2000a] have identified the catchment of the Wadi al-Dahal as the source of this fan. The area of this basin is 97 km^2 and the fan itself is much smaller than the alluvial surfaces that can be found in the central section of the valley. Consequently, we have to consider basins larger than ~100 km^2. The seven basins of such size are marked on Figure 3. Obviously, the Wadi Abu Burqu' and the Wadi Rakiya cannot be the sources of the large alluvial surfaces, as they are located south of them: it would contradict the left-lateral sense of motion of the Dead Sea fault. Five possible sources remain, from north to south: the Wadi Qala, the Wadi Khunayzira, the Wadi Fidan, the Wadi Huwar, and the Wadi Musa. In section 6.2, we propose a possible pairing of each alluvial surface with a catchment source, based on a detailed geomorphic analysis and a series of ^{10}Be CRN model ages.

4. Detailed Morphotectonic Analysis of the Large Alluvial Fans

4.1. The Risha and al-Dhawi Alluvial Fans

[15] The site of Risha is located at the center of the Wadi Araba, and is marked by the ridge of the Jabal al-Risha (the term "jabal" meaning hill here) (Figures 3 and 4). This ridge is elongated along the WAF and asymmetric, with steep slopes to the east and gentler slopes to the west. The central part of the ridge stands 100–150 m above the valley floor, with the elevation decreasing southward. This local uplift is explained by the slight change in the fault azimuth, from a N14°E left-lateral strike-slip segment to the north, to N17°E along the ridge. A secondary reverse fault, located to the west of the ridge, also attests to the transpressive component [*Garfunkel et al.*, 1981]. The ridge is formed of a poorly indurated conglomerate, the Risha Gravel, Pleistocene in age [*Barjous*, 2003], which appears to be folded, as observed in the field and reported on our interpretative cross section (Figure 4d).

[16] The northern and central parts of the ridge have a different appearance. The northern part is fairly flat and relatively preserved from gullies incision. It is darker in color (Figure 4e). Contrary to the geological maps, where it has been mapped as the Risha Gravel [e.g., *Barjous*, 1995; *Sneh et al.*, 2000], our observations show that this part of the

ridge is covered by more recent alluvium that unconformably overlies the Risha Gravel (Figure 4d).

[17] Two large alluvial fans, which shapes are well defined by radial topographic contour lines, rest to the west of the ridge. Both fan apices are uplifted relative to the valley floor, thus both alluvial surfaces are inactive today. These two fans of similar size lie side by side. Deeper surficial incision into the southern fan suggests that it is the oldest. This is also supported by evidence for slight lateral erosion of the southern fan when the northern fan was emplaced (see white circle on Figure 4b). Based on ^{10}Be CRN ages, the southern fan surface corresponds to level F5 and the northern one to F3c.

[18] The apex of F5 is fairly wide and partly occupied by Al-Risha village, hampering any precise location. The proximal part of the fan is down dropped relative to the distal part along a secondary fault, which scarp faces to the east. While the radial topographic contour lines at the distal part of the fan converge to the center of the apex, contour lines on the down dropped part rather converge to the northern rim of the apex. This observation would be consistent with tilting of the apex, related to a southward decreasing uplift.

[19] By contrast, the apex of the northern fan F3c is clearly incised within the ridge. It is narrow, ~250 m wide, with an oblique direction relative to the fault. F3c is inset into the flat northern part of the ridge that is thus older and mapped as F4, the timing of deposition relative to F5 being determined from ^{10}Be CRN ages (section 5.2.1). South of F4, a small surface ~1 m lower than F4 and that appears less incised on satellite views was mapped as F3b. It stands ~4 m higher than F3c. The extent of the surface F4 to the north remains uncertain. North of the sampling site (f), the elevation of the surface gently decreases to reach another flat area that is ~10 m lower than F4. This surface is probably younger than F4, possibly corresponding to a late F4 stage or to an early F3 stage. We later refer to this surface as F3a. The distal part of the fan F3c is limited to the north by a riser that separates F3c from two lower and light colored (thus younger) incised alluvial surfaces, which are mapped as F2 and F1.

[20] Across from the Jabal al-Risha, east of the fault, is the outlet of the Wadi Huwar, one of the largest catchments draining the Jordanian Plateau toward the Wadi Araba (Figure 3; section 3). Its riverbed is narrow and deeply incised in the bedrock, with a large alluvial fan, light in color, emplaced at its mouth. Most of the surface F0 is active, with only few abandoned lobes mapped as F1. Abandoned surfaces, F2 or older, are visible on both sides of the active fan. The present-day stream and the morphology of these abandoned surfaces attest to water flowing both northward and southward, although the main flux seems to be directed to the north in the most recent time. The direction of flow, however, has probably evolved coincidentally with

Figure 4. (a) SPOT5 satellite image of the Risha site. (b and c) Morphotectonic map of the Risha site over SPOT5 satellite image in Figure 4a. Topographic contour lines are from 1:50,000 topographic maps and SRTM3 data. White circle points out evidence for lateral erosion of F5 when F3c was emplaced (see text). AA′ white dashed line shows location of the interpretative cross section in Figure 4d. B points to the outcrop location of N35°E dipping beds of Risha Gravel. (d) Interpretative cross section. (e) Oblique high-resolution Google Earth view of the northern part of the site. Red arrows delineate the fault. Note the difference in color, relief and incision of the ridge, north and south of the apex of F3c. Letters refer to sampling sites (see Table 1).
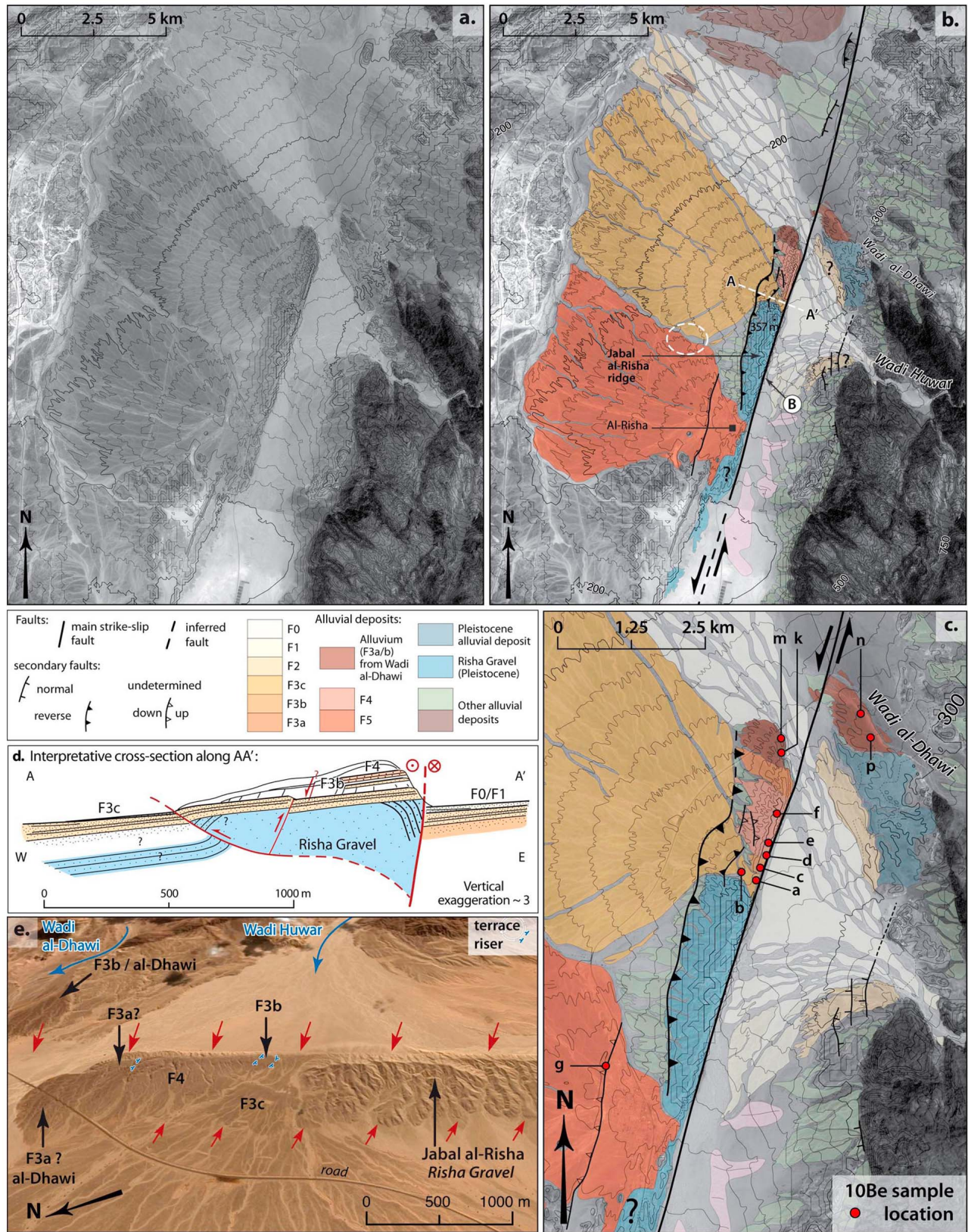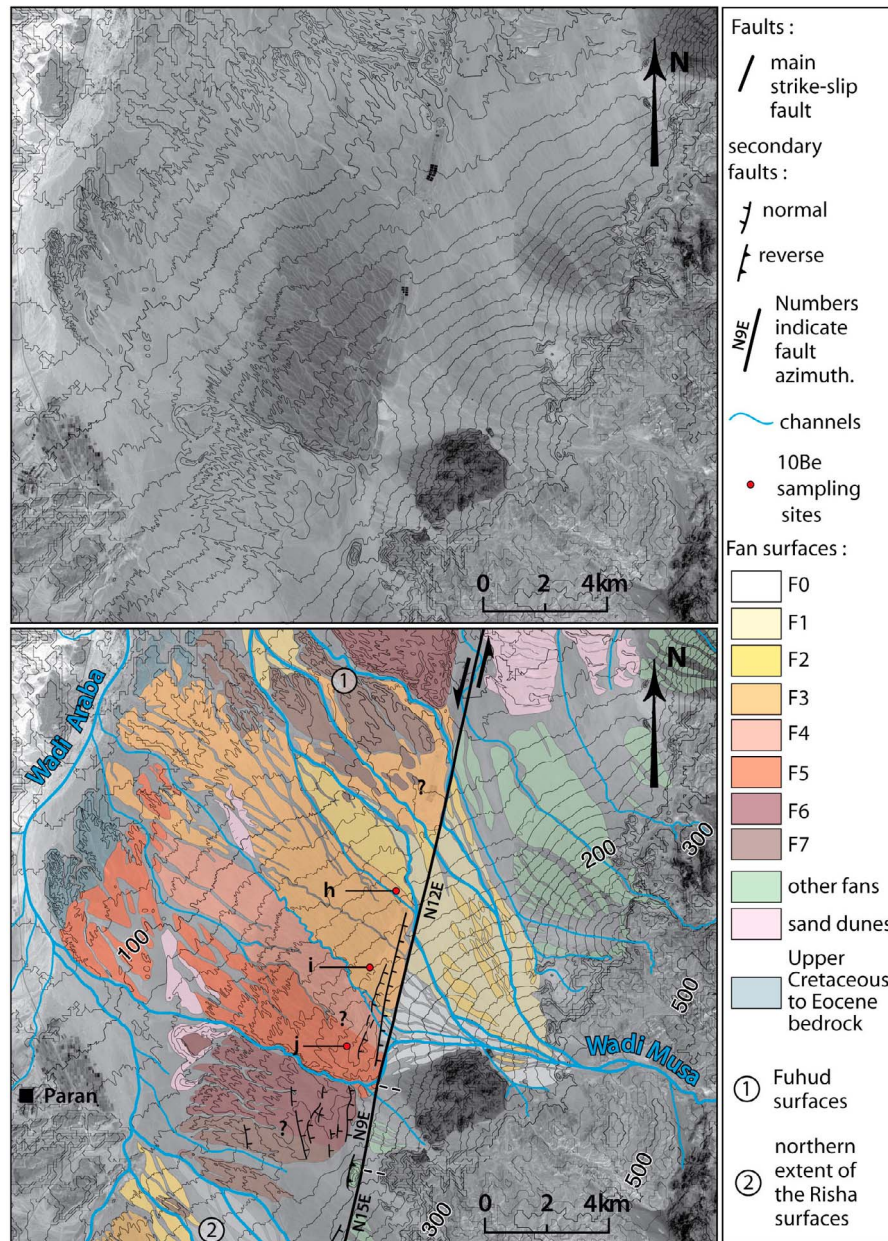
Figure 4

Figure 5. Morphotectonic map of the site of Mazla over SPOT5 satellite image. Topographic contour lines have been digitized from 1:50,000 topographic maps. Letters refer to sampling sites (see Table 1).

the uplift and the left-lateral displacement of the Jabal al-Risha, which prevents the stream to flow directly westward.

[21] The alluvial units found at the northern tip of the Jabal al-Risha are clearly distinct from the alluviums located further south along the ridge. The northernmost unit lies 10–15 m lower than F4, at about the same elevation as the lower surface F3a. This unit exhibits a characteristic darker paved surface (Figure 7) and it is mostly composed of dark color angular pebbles embedded into a peculiar reddish sandy matrix. Hence, this dark alluvium originated from a drainage that differs from the source of the other deposits found in Risha, where light color pebbles and cobbles embedded in a

beige sandy matrix dominate (Figure 7). This distinct reddish surface is more deeply incised than F4. The transition between the reddish surface and the surface F3a to the south is gradual with a ~30 m wide interfingering zone, visible in the numerous gullies incising the area. The northeastern riser of the ridge, constantly rejuvenated by the wash, shows evidences for occasional mixing of lighter material with the reddish dark conglomerate in this area. This advocates for contemporaneous emplacement of the surface F3a and the northern reddish surface, and thus it has been eventually mapped as F3a. The deeper incision into the northern surface is interpreted as an effect of the abrupt drop between this
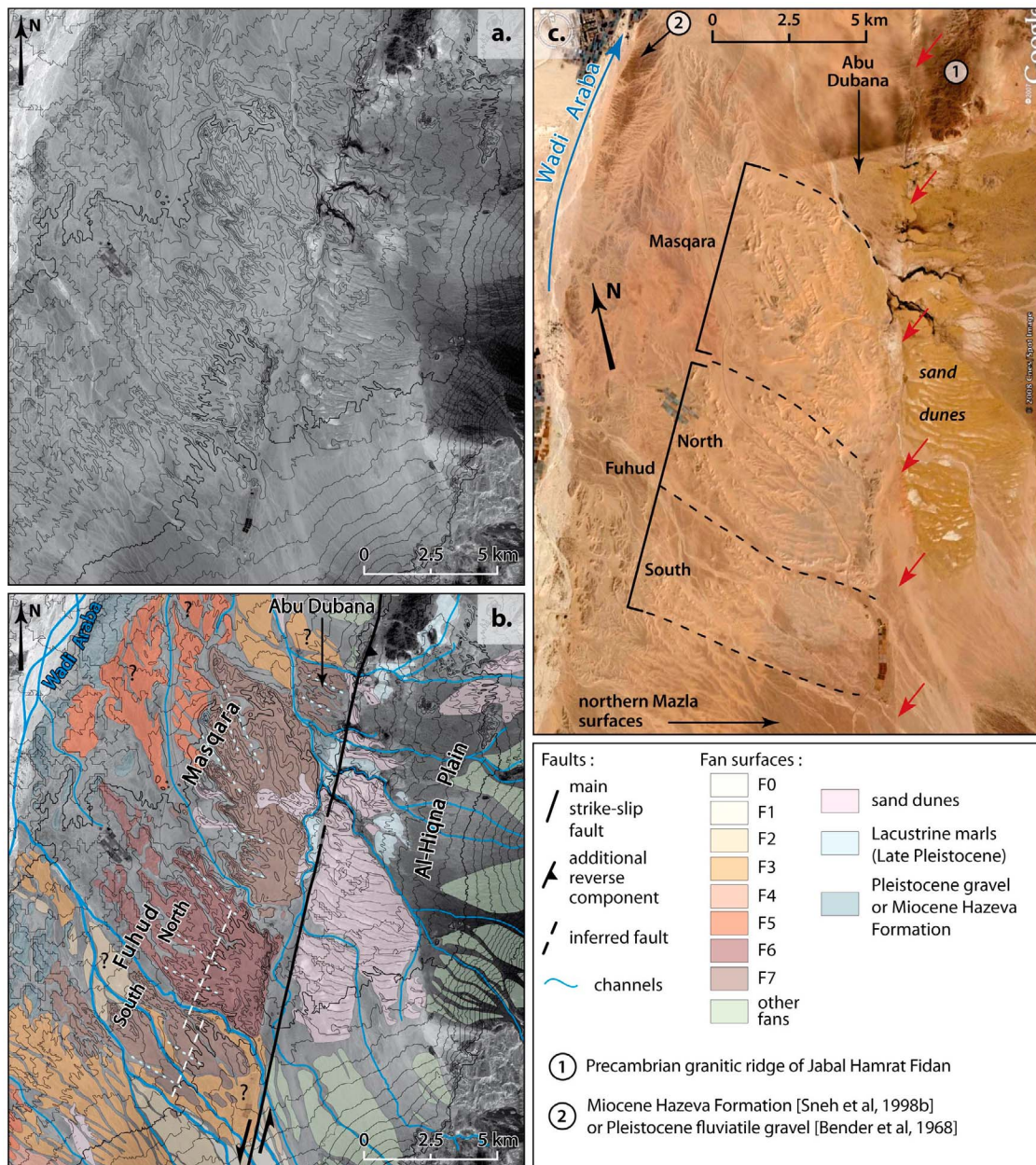
Figure 6. (a) SPOT5 satellite image. (b) Morphotectonic map of the Fuhud and Masqara surfaces over SPOT5 satellite image in Figure 6a. Topographic contour lines have been digitalized from 1:50,000 topographic maps. White dashed line on the Fuhud surfaces show that topographic contour lines, taken at the preserved top part of the alluvial surface, can be fitted by a straight line, attesting to a distal source for the deposits. Dotted lines indicate the incision pattern. (c) High-resolution Google Earth view of the surfaces.

surface and the lower level F1, while the transition from F4 to F1 is more gradual, through F3c.

[22] North of the Jabal al-Risha and east of the fault, an abandoned alluvial surface shows the same characteristic darkness, clast composition, and unmistakable reddish sandy matrix as the surface located west of the fault at the northern tip of Jabal al-Risha. Hence, it strongly suggests that both alluviums were part of the same deposit. Since this surface is deposited at the Wadi al-Dhawi outlet, we later refer to it as the al-Dhawi fan.

4.2. The Mazla Alluvial Fans

[23] At Mazla, we observe a series of abandoned alluvial deposits sharply limited to the east by the active trace of the WAF (Figure 5). The fault trace is mostly straight and it is expressed as a single strand striking N12°E. Local changes in the fault azimuth, however, are responsible for secondary normal faulting affecting the alluvial surfaces located west of the WAF and for the growth of a 1 km long push-up structure in the southern part of the site. West of the fault, the alluvial

surfaces gently sloping ∼1°W extend until the thalweg of the Wadi Araba, along the western valley edge. Higher elevation and deep incisions by several westward flowing drainages attest to the uplift of the western side relative to the eastern one, possibly related to the small transtensive component on a slightly east dipping fault plane.

[24] West of the fault, we have identified seven successive levels of alluvial surfaces (F7 to F1) above the present-day channel, which appearances evolve from south to north (Figure 5). Moving northward, the elevation (taken at the easternmost part of the surfaces) decreases and the topographic contour lines attest to a lower degree of incision of the surfaces. The successive surfaces also become lighter in color to the north, suggesting a northward decrease of the age of the surfaces. Surfaces F6 and F7 depart from this general pattern, as they appear to be the lightest in color. We attribute this light color to a poorer preservation of the top part of F6 and F7, due to surface incision by regressive rills and associated surface deflation. The distal parts of the surfaces, to the west, are all lighter on the SPOT5 image because they are sprinkled with sand. From south to north the orientation of the topographic contour lines also varies. To the south, on surfaces F7 and F6, the steepest slope is oriented N80°W westward. It rotates gradually to reach a northwest orientation (N40°W) for F3 and F2. North of F2, the slope of the high and deeply incised surfaces of the Fuhud site (Figure 6), which morphology appears to be similar to the one of surfaces F6 and F7, is oriented westward again.

[25] East of the fault the main feature is the large alluvial fan emplaced at the mouth of the Wadi Musa, one of the largest eastern tributaries of Wadi Araba (see section 3). A massive outcrop of Precambrian volcanic rocks [*Barjous*, 1995] (black in color) bounds the riverbank of Wadi Musa to the south. Satellite images and topographic contour lines show that the influx of dark volcanic clasts is actually very small compared to the light-in-color clasts contribution from the surrounding catchments, and it could not be held responsible for the dark color of the western surfaces, which is related to the development of the desert varnish and pavement.

[26] Two parts can be distinguished on the Wadi Musa fan, east of the fault. The bright southern part is the most active part today. It is characterized by radial topographic contour lines defining a smaller alluvial fan inset in the large-scale fan. This deposit originated from water flowing N75°W, straight out of the mouth of the wadi, before diverging ∼3 km downstream from the outlet. The northern part of the fan seems slightly older, from its darker color and the surficial incision by a few drainages. Topographic contour lines attest to a water flow oriented toward the northwest. Two levels of alluvial surfaces can be observed above the present-day streams. The surface F1 may be followed on the western side of the fault, blanketing the inset channels. The surface F2, more patchy, is more incised and a little darker than F1. Because the toe of the eastern alluvial fan abuts on the higher deposits located west of the fault (F2 to F7), the fan geometry has probably evolved considerably through time, depending on the path found by the water flow to cross or get around the obstacle. The dog-legged geometry of most drainages attests to it. They have either been left-laterally offset by the fault, or they flow along the fault to

capture an abandoned drainage and find a way out further toward northwest.

4.3. The Site of Fuhud and Masqara

[27] The configuration of this site is quite similar to the one of Mazla (Figure 6). Large abandoned alluvial surfaces, deeply incised, are dipping westward. They are bounded sharply to the east by the linear active trace of the WAF. Slight uplift of the western block probably also takes place here. Unlike at the site of Mazla, all the surfaces exposed west of the fault seem to be fairly old: they are ∼20 m high above the present-day streams, densely incised, and light in color due to surface degradation from regressive incision and deflation.

[28] The northern and southern surfaces of Fuhud have a very similar appearance to, respectively, the surfaces F6 and F7 of Mazla. The northern surface is slightly darker and a larger area of its top part surface remains (Figure 6c), so that it may be a little younger than the southern surface. Yet, both surfaces have similar elevation. The topographic contour lines of both surfaces could fit straight lines, suggesting a remote source for these deposits. The southern surface is composed of several patches surrounded by a lower and darker surface inferred as F3.

[29] The surface of Masqara, located just north of Fuhud, has a different appearance. Although the lighter color seems related to sand cover (Figure 6c), the surface is clearly more incised. In addition, the elevation of the eastern part of the surface significantly decreases northward, from ∼80 m to ∼10 m. The highly curvy topographic contour lines on this surface make it difficult to assess a comprehensive pattern of emplacement, or incision. However, incised rills tend to be oriented from ∼N70°W in the south to N20°W in the north. The relative chronology of deposition between this surface and the northern Fuhud surface could not be established due to the bad preservation of surfaces and the presence of sand dunes hiding the contact between the two surfaces.

[30] The Masqara alluvium is bounded to the north by a small alluvial surface, the Abu Dubana alluvium, probably of similar age since it exhibits a similar degree of incision. This surface is significantly lower in elevation, at ∼15 m bsl, than the Masqara surface. Unlike for the Masqara surface, the topographic contour lines corresponding to the Abu Dubana alluvium are parallel to the fault trace.

[31] The area east of the WAF, the al-Hiqna Plain, consists of coalescent west dipping alluvial fans and of a large sand dunes field. The alluvial deposits seem to be much younger than to the west, since the fans are still active and the oldest abandoned alluvial deposits exhibit well-preserved dark surfaces with shallow incision. Also reported on the 1:50,000 geological map [*Rabb'a*, 1991, 1994], late Pleistocene lacustrine marls that appear as bright spots on the satellite images are overlaid by the alluvial deposits, supporting late Pleistocene or younger ages.

5. Surface Exposure Dating of the Abandoned Alluvial Surfaces

5.1. Analytical Approach

[32] Abandoned alluvial surfaces can be dated using CRN surface exposure dating techniques [*Lal*, 1991; *Gosse and Phillips*, 2001]. In this study, we use ^{10}Be cosmogenic

Table 1. [10]Be CRN Dating Data: Sample Information, [10]Be Concentrations, and Model Ages[a]

Surface	No.	Sample	Lithology[b]	Location[c] (°N/°E)	Elevation (m)	[10]Be Concentration (×10^{4} atoms/g SiO$_2$)	±Error (×10^{4} atoms/g SiO$_2$)	Minimum Age[d,e]	Int ±[f]	Ext ±[f]	Maximum Age[d,e]	Ext ±[f]	Percent[g]
Risha site													
F3c	1	RA06-3	gr	30.261421/35.237881 (a)	300	22.81	0.64	48.6	1.4	4.5	53.1	5.4	9
	2	RA06-6C	a. rd qtz	30.261421/35.237881 (a)	299	30.67	0.76	64.0	1.6	5.9	72.1	7.6	13
	3	RA06-1	gr	30.261450/35.237521 (a)	297	31.70	0.71	66.9	1.5	6.1	76.0	8.0	14
	6	RA06-5	qtzite	30.261473/35.237762 (a)	300	35.01	0.89	75.6	2.0	7.0	87.6	9.5	16
	7	RA06-2	gr	30.261370/35.237699 (a)	299	37.21	0.80	79.2	1.7	7.2	92.6	10.0	17
	8	RA06-4	qtzite	30.261457/35.237916 (a)	298	53.64	1.19	116.3	2.6	10.7	148.8	18.3	28
	4	RA06-34C	a. rd qtz	30.262670/35.234913 (b)	281	32.26	0.82	68.3	1.8	6.3	77.6	8.2	14
	5	RA06-33	qtzite	30.262670/35.234913 (b)	281	33.75	0.86	73.6	1.9	6.8	84.9	9.2	15
	9	RA06-31	qtzite	30.262617/35.234946 (b)	281	58.87	1.72	128.6	3.9	12.2	170.3	22.5	32
F3b	10	RA06-14C	a. rd qtz	30.263109/35.238564 (c)	306	47.97	1.71	100.5	3.7	9.7	122.9	14.9	22
	11	RA06-8	qtzite	30.263039/35.283990 (c)	306	75.88	1.99	162.7	4.4	15.4	240.1	36.8	48
	12	RA06-11	qtzite	30.263109/35.238564 (c)	305	115.39	2.22	255.3	5.3	24.2	641.6	272.6	151
F4	13	RA06-29C	a. rd qtz	30.264344/35.239143 (d)	304	72.62	1.70	154.1	3.8	14.4	218.5	31.2	42
	14	RA06-26C	a. rd qtz	30.264909/35.239293 (e)	307	67.60	1.59	143.0	3.5	13.3	195.5	26.5	37
	-	RA06-23C	a. rd qtz	30.266977/35.239961	311	_h	-	-	-	-	-	-	
	15	RA06-16	qtzite	30.271202/35.241534 (f)	312	69.08	1.63	150.6	3.7	14.1	213.3	30.5	42
	16	RA06-19C	a. rd qtz	30.271202/35.241534 (f)	313	85.44	2.36	181.7	5.3	17.3	284.7	48.2	57
	17	RA06-17	qtzite	30.271192/35.241529 (f)	312	83.31	2.03	183.2	4.7	17.3	292.1	50.4	60
F5	18	RA06-36C[i,j]	qtzite	30.233337/35.210312 (g)	251	126.30	2.97	301.9	7.7	29.3			
	19	RA06-38C[i,j]	a. rd qtz	30.233337/35.210312 (g)	251	131.99	3.10	302.8	7.7	29.4			
	20	RA06-35[i,j]	qtzite	30.233299/35.210309 (g)	251	144.85	3.40	344.2	8.8	33.8			
Wadi al-Dhawi site													
F3a west of fault	D2	DW09-2	a. rd qtz	30.28160/35.243281 (k)	267	59.33	1.73	128.9	3.9	12.2	169.7	22.2	32
	D2a	DW09-2a	qtz	30.28160/35.243281 (k)	267	48.31	1.41	106.0	3.2	10.0	131.4	15.8	24
	D2b	DW09-2b	a. ang qtz	30.28160/35.243281 (k)	267	73.90	2.10	163.2	4.8	15.5	238.7	36.4	46
	D4	DW09-4	a. rd qtz	30.28325/35.242781 (m)	262	63.52	1.89	139.4	4.3	13.3	189.2	25.9	36
	D5	DW09-5	qtz	30.28325/35.242781 (m)	262	56.88	1.65	125.9	3.8	11.9	164.4	21.2	31
	D5a	DW09-5a	a. rd qtz	30.28325/35.242781 (m)	262	60.35	2.04	132.2	4.6	12.7	175.7	23.7	33
	D8	DW09-8	a. ang qtz	30.28581/35.256510 (n)	273	51.86	1.50	112.11	3.3	10.6	141.1	17.3	26
	D9	DW09-9	a. rd qtz	30.28581/35.256510 (n)	273	48.57	1.57	104.4	3.5	9.9	128.9	15.6	23
	D12	DW09-12	a. ang qtz	30.28315/35.258389 (p)	278	50.52	1.65	109.2	3.7	10.4	136.4	16.8	25
	D13	DW09-13	a. rd qtz	30.28315/35.258389 (p)	278	49.31	1.44	105.6	3.2	9.9	130.8	15.7	24
Mazla site													
F3	21	MA06-3	rhyo	30.420323/35.278760 (h)	156	18.94	0.64	44.4	1.5	4.2	47.8	4.9	8
	22	MA06-1	gr	30.420408/35.278828 (h)	155	21.79	0.52	51.1	1.2	4.7	56.1	5.7	10
	23	MA06-4C	a. rd qtz	30.420323/35.278760 (h)	156	34.94	0.82	81.5	2.0	7.5	95.1	10.4	17
	24	MA06-2	rhyo	30.420303/35.278703 (h)	157	34.58	1.01	81.8	2.4	7.7	94.6	10.4	16
	25	MA06-7	qtzite	30.399413/35.269219 (i)	175	39.42	0.76	93.4	1.8	8.5	112.6	12.7	21
	26	MA06-6	qtzite	30.399389/35.269344 (i)	175	51.34	1.21	104.5	3.0	9.8	129.3	15.5	24
	27	MA06-8C	a. rd qtz	30.399389/35.269344 (i)	175	44.63	1.26	119.1	2.9	11.1	152.2	18.8	28
	28	MA06-5	qtzite	30.399349/35.269351 (i)	175	105.86	2.47	258.4	6.4	24.8	648.5	279.6	157
F5	29	MA06-12C[d,j]	a. rd qtz	30.376626/35.261067 (j)	196	130.21	4.13	311.7	10.7	31.2			
	30	MA06-11[i,j]	qtzite	30.376593/35.261130 (j)	196	130.58	3.90	318.5	10.3	31.7			
	31	MA06-9[i]	qtzite	30.376700/35.261278 (j)	196	131.17	3.81	328.4	10.4	32.7			
	32	MA06-10[i]	rhyo	30.376626/35.261067 (j)	197	145.34	3.47	362.3	9.5	35.8			

radionuclide. The concentration of ^{10}Be isotopes of a rock sample mostly depends on the exposure time of the rock to cosmic rays, on the erosion rate of the surface, and on an inheritance component due to possible exposure of the cobble prior to its final deposition [*Lal*, 1991]. In this study, CRN samples were prepared using the procedure of *Kohl and Nishizumii* [1992] and model ages were calculated using the CRONUS-Earth calculator v2.2 [*Balco et al.*, 2008], using the constant production rate scaling scheme from *Lal* [1991] and *Stone* [2000]. More details regarding samples processing and age calculation are provided in *Le Béon et al.* [2010], Table 1, and auxiliary material Data Set S1.[1]

[33] We targeted sampling sites located on well-preserved alluvial surfaces at the sites of Risha, al-Dhawi, and Mazla (Figures 3b, 4, 5, and 7). At each site we collected 3 to 9 rock samples, well embedded in the surface to ensure their long-term stability [e.g., *Ryerson et al.*, 2006]. At Risha and Mazla we sampled cobbles because they are the most representative clast size on the surfaces. Various quartz-rich lithologies (Table 1) have been collected: granite, quartzite, and rhyolite. Amalgamated samples of 15 to 20 rounded quartz pebbles of similar size (2–3 cm) were collected in parallel. Such samples are expected to represent an average of the clast population and may help gain a better understanding of the exposure history of the clasts by comparison of their age to those of individual cobbles [*Hetzel et al.*, 2002; *Matmon et al.*, 2009]. At each sampling site, the correction for shielding of cosmic rays related to the surrounding topography was found to be negligible.

[34] When computing CRN ages, we assumed that pre-exposure on the cliffs and during transport and possible storage in the drainage basin [*Anderson et al.*, 1996; *Repka et al.*, 1997] is negligible. The sources of the deposits we are interested in are large catchments (>150 km^2) with characteristic lengths of 15–20 km. The drainages are fairly steep and narrow, incised in the bedrock, therefore with limited clasts storage. Since we sampled various lithologies coming from different locations in the catchment, inheritance, if any, is expected to be scattered rather than constant and dependent on lithology. This aspect will be discussed in the light of the age distributions in section 5.2.

[35] Arid environments usually show highly preserved landscapes. Desert pavement developed at the surface of

alluvial deposits may protect them from erosion and deflation [*Wells et al.*, 1995; *Quade*, 2001; *Regard et al.*, 2006; *Van der Woerd et al.*, 2006]. Successful exposure dating up to ~2 Ma of clasts from the pavement of abandoned alluvial surfaces in the eastern Negev [*Matmon et al.*, 2009; *Guralnik et al.*, 2010], just west of the Wadi Araba, attest for high surface preservation. A low maximum erosion rate of 0.3 m/Ma was derived from the oldest of these surfaces [*Matmon et al.*, 2009]. Preservation of the desert varnish and desert pavement at our sites suggest that the effect of erosion is small for the surfaces targeted for dating (F3 to F5). However, the light color of the oldest surfaces F6 and F7 (section 4, Figures 5 and 6) attests to a significant effect of erosion at longer timescale, probably once regressive erosion has reduced the flat top part of the surface to a given threshold. To test our field-based hypothesis, we used our ^{10}Be data to calculate a maximum erosion rate. We assumed that enough terrace material has been removed by erosion to justify the steady state erosion model [*Lal*, 1991] (i.e., production is balanced by radioactive decay) for the samples with the highest ^{10}Be concentrations, the samples from the fans F5 at Risha and Mazla (Table 1). Using a value of 160 g/cm^2 for the attenuation length and the rock samples density (Table 1), we obtained a maximum erosion rate of 2.1 ± 0.1 m/Ma. Because the study area experiences uniform climatic conditions and because the configuration of our sites is similar, we can reasonably apply the same erosion rate at all sites presented here. This clearly is a conservative approach, since the maximum erosion rate derived by *Matmon et al.* [2009] is 10 times lower. For each sample, the minimum and the maximum ages (calculated assuming no erosion and maximum erosion, respectively) are given in Table 1. For ages in the order of 70 ka, maximum erosion would lead to a 15% increase of the age, which is barely larger than the uncertainty, confirming the zero-erosion hypothesis for surfaces F3 and younger [e.g., *Ryerson et al.*, 2006]. The maximum erosion rate would imply very poor age control for surfaces older than F4. An erosion rate of 0.3 m/Ma would have negligible effect on any CRN age, even from surface F5, for which the increase in age would remain within 10%. In the following, we consider the minimum ages to discuss our results.

[36] CRN dating of alluvial surfaces may not only be biased by preexposure and erosion, but also by the complexity of alluvial processes (e.g., duration of surface activity, postdepositional contamination related to exceptional flood events) and by postdepositional processes on the

---

Notes to Table 1:

[a]The complete set of analytical parameters required for age calculation is available as auxiliary material (Data Set S1). No. corresponds to number used in maps and graphs.

[b]Densities of 2.7, 2.65, and 2.5 g/cm^3 were used for granite, quartzite/quartz and rhyolite samples, respectively. Lithologies: gr = granite, qtzite = quartzite, rhyo = rhyolite, amalgamated samples: a. rd qtz = rounded quartz pebbles, a. ang qtz = angulous quartz pebbles.

[c]Letters in parentheses indicate sampling sites shown in Figures 4 and 5.

[d]Model ages were calculated with the CRONUS-Earth online calculator, version 2.2 [*Balco et al*, 2008] (http://hess.ess.washington.edu/math). Calculator uses the revised value of (1.36 ± 0.07)E6 years for the ^{10}Be half-life [*Nishiizumi et al.*, 2007].

[e]Minimum model age, calculated with no erosion ; Maximum model age, calculated with maximum erosion rate of 2.1 m/Ma.

[f]Int/Ext ±, internal/external uncertainty. The internal (or analytical) uncertainty includes error from the blank and the AMS counting statistics. The external (or propagated) uncertainty takes into account uncertainty in the production rate and scaling factors.

[g]Percent, ratio of model age calculated assuming a given erosion rate over minimum model age.

[h]Too high boron at AMS.

[i]Sample used to compute an average maximum erosion rate of 2.1 ± 0.1 m/Ma.

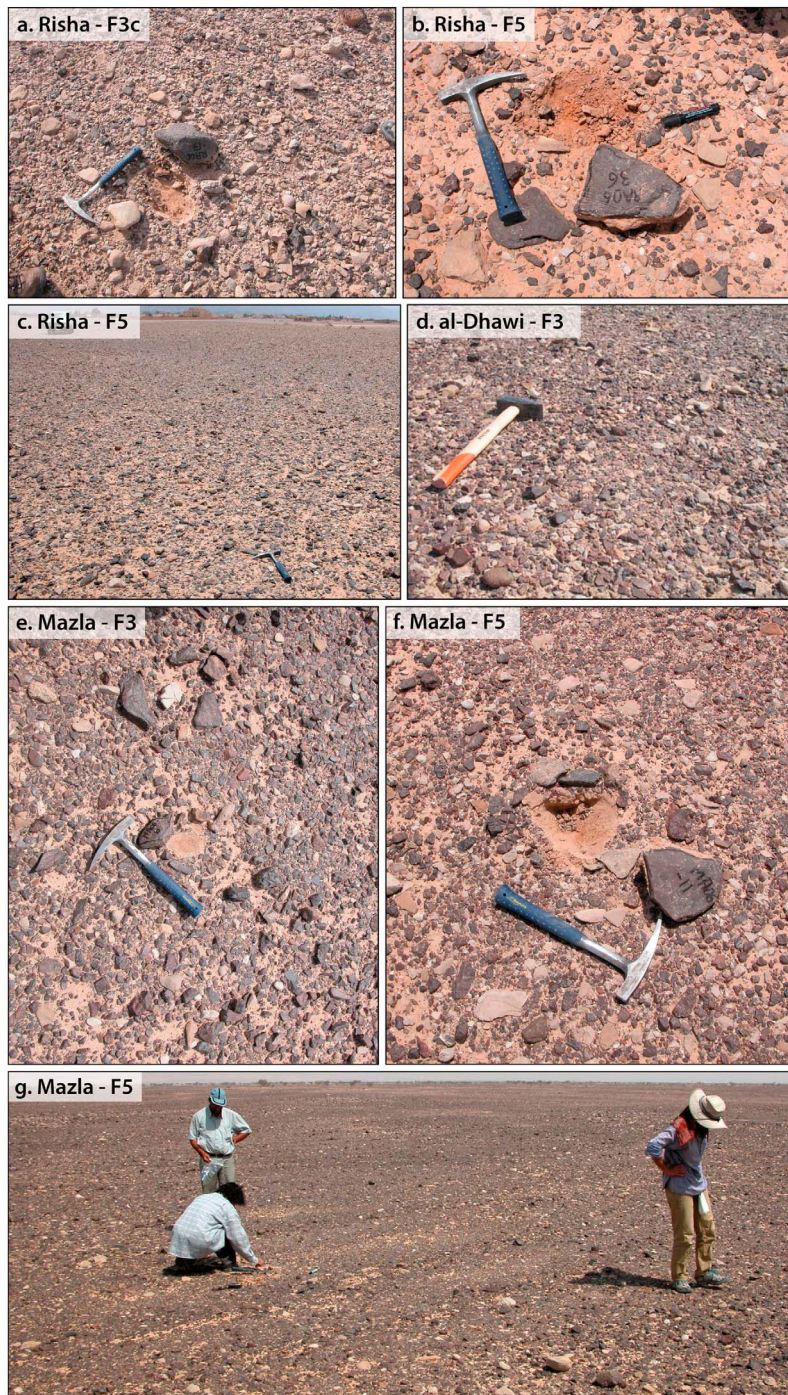[j]Saturation reached. Undetermined age > several Ma.

Figure 7. Sampling at the sites of Risha, al-Dhawi, and Mazla. Site locations are shown on Figures 4 and 5. (a) Sample RA06-33 collected at Risha on surface F3c (site b). (b) Sample RA06-36 on surface F5. (c) View of the surface F5 at Risha where sample RA06-36 was collected (Site g). (d) View of the al-Dhawi surface F3, west of the fault (site k). (e) View of the paved surface F3 at Mazla, at the location of sample MA06–6 (site i). (f) Sample MA06–11. (g) View of the surface F5 at Mazla (site j) where sample MA06–11 was collected.

geomorphic surface [e.g., *Bull*, 1991]. All such processes may result in scattered age distribution. The definition of age clusters and the rejection of outliers are often arguable, especially in small data sets [e.g., *Van der Woerd et al.*, 1998; *Mériaux et al.*, 2004, 2009; *Ritz et al.*, 2006; *Le Béon et al.*, 2010]. In this study, we reject visually obvious outliers and define clusters from the other ages, even if they do not compare within internal uncertainty. For each surface we calculated from the minimum CRN model ages, the weighted
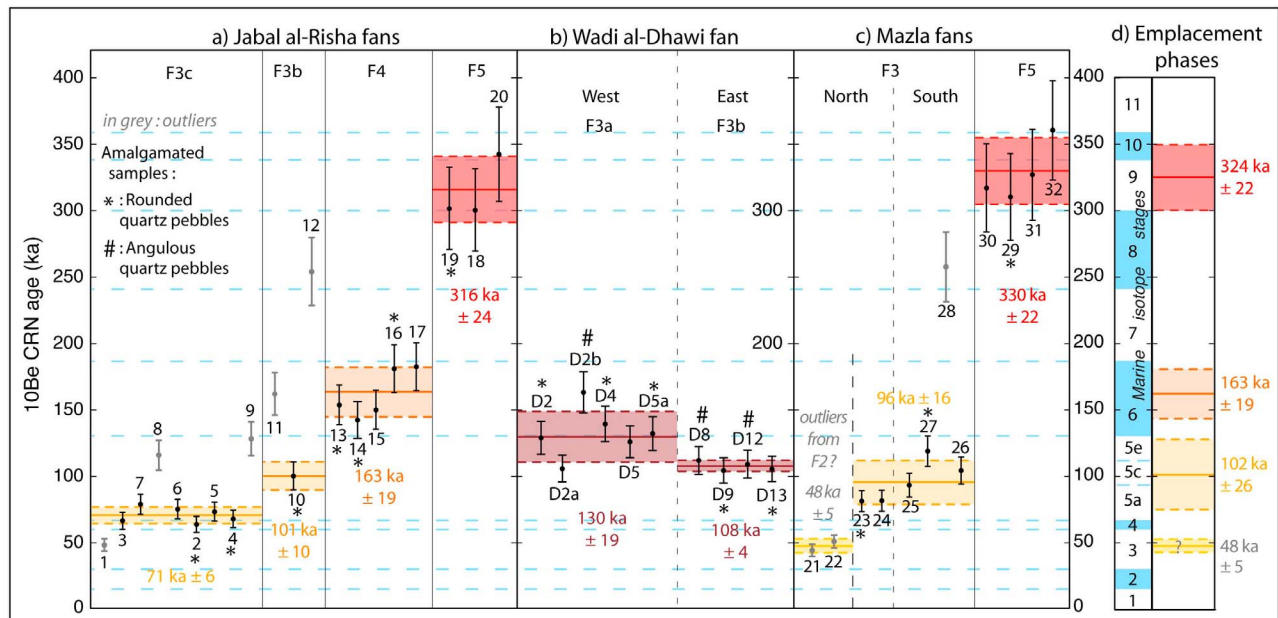
Figure 8. Distribution of the [10]Be CRN model ages at the sites of (a) Risha, (b) al-Dhawi, and (c) Mazla and (d) synchronous emplacement phases of alluvium.

mean age, applying weights that depend on the normalized internal uncertainty, and the standard deviation σ.

5.2. Results

5.2.1. The Risha Site

[37] At Risha, we sampled the northern fan F3c, the northern part of the ridge covered by F3b and F4, and the southern fan F5 (Figure 4). The surfaces at the sampling sites are characterized by their flatness, their dark color and the desert pavement, which all indicate that the surfaces have not been modified recently either by natural erosion, animals or human activity (Figure 7). Ages are shown in Table 1 and on Figure 8.

[38] On the fan F3c, we collected nine samples in total from two locations near the apex. Six exposure ages (including ages derived from the amalgamated samples) are clustered between 64 ± 6 ka and 79 ± 7 ka, one is significantly younger (49 ± 5 ka, sample 1) and two are significantly older, 116 ± 11 ka (sample 8) and 129 ± 12 ka (sample 9), which are probably related to a more complicated exposure history than a single phase of deposition and abandonment. The presence of older samples can be explained by inheritance, related to remobilization of older deposits located upstream, and/or to preexposure in the catchment. Discarding these samples, we obtained an average exposure age of 71 ± 6 ka based on six samples.

[39] North of the apex of F3c, we collected two cobbles and an amalgamated sample on F3b and five amalgamated samples in total from three locations on F4. On F3b we obtained scattered exposure ages: 101 ± 10 ka (sample 10) for the amalgamated sample and 162 ± 15 ka (sample 11) and 254 ± 24 ka (sample 12) for the two cobbles. On F4, the five samples yielded consistent ages between 143 ± 13 ka and 183 ± 17 ka. The agreement between ages from amalgamated samples and from most individual cobbles at our

sites as well as in previous studies [e.g., *Le Béon et al.*, 2010; *Schmidt et al.*, 2011], supports the reliability of the amalgamated samples to provide an appropriate estimate of the exposure age of the surfaces. Hence, regarding surface F3b, we give more confidence to the age of the amalgamated sample 10 than to the ages of individual cobbles that could be explained by inheritance during transport or as reworked material from older deposits (possibly F4 for sample 11). We then considered an age estimate of 101 ± 10 ka (sample 10) for F3b and an average age of 162 ± 19 ka from the five samples on F4.

[40] To the south, on the fan F5, we collected two cobbles and an amalgamated sample of rounded quartz pebbles. Due to the vicinity of the village of Al-Risha, we targeted a site as close to the fan apex as possible, yet away from gravel quarries and car tracks. We obtained two ages at 302 ± 29 ka (amalgamated sample) and 303 ± 29 ka, and one at 344 ± 34 ka. We computed an average age of 316 ± 24 ka for F5. This estimate should be considered with care, given the small number of samples collected at only one location and the possibly significant effect of erosion processes (if >0.3 m/Ma; see section 5.1) for this surface.

[41] On F3c and F4, the age distributions are relatively clustered, especially for F3c. Outliers are considerably older than the cluster of ages and their number is limited. Interestingly, they are all quartzite cobbles that come from further up in the catchment than granites. Yet, other quartzite cobbles (samples 5 and 6 on F3c and samples 15 and 16 on F4) agree with the age cluster. The consistency between the ages derived from cobbles of different lithologies and amalgamated pebbles suggest that average inheritance is likely to be small. Occasional large inheritance of quartzite cobbles might be due to preexposure in the catchment cliffs, although remobilization of late Quaternary deposits located upstream remains possible.

5.2.2. The Al-Dhawi Site

[42] At al-Dhawi, cobbles of quartz-rich lithologies were scarce (Figure 7). We mostly collected amalgamated samples of quartz pebbles from flat paved surfaces away from gully incisions at two locations on both sides of the fault (Figure 4 and Table 1). West of the fault, we also collected two small quartz cobbles. The pebbles were sorted between rounded ones and angular ones, to test for the effect of duration of transport and possible postabandonment processes at the surface of the deposit, such as fracturing of cobbles.

[43] The age distributions that we obtained on either side of the fault differ from each other. East of the fault, the four ages are consistent within the narrow range of 104 ± 10 ka (D9) to 112 ± 11 ka (D8) and average to 108 ± 4 ka. West of the fault, the ages are generally slightly older and more scattered. Four samples cluster from 126 ± 12 ka to 139 ± 13 ka; one is slightly younger (106 ± 10 ka, D2a) and one slightly older (163 ± 16 ka, D2b). They yield an older average age of 130 ± 19 ka. Except for sample D2b, no significant age difference is observed between samples composed of rounded or angular pebbles. This suggests that the effect of duration of transport, clast abrasion during transport, and postabandonment processes are negligible or balanced.

[44] While the eastern and western surfaces were proposed to be of same age, the average ages only slightly overlap. The western surface being older could be explained by an earlier abandonment of this surface as it is uplifted and moved away from the feeding catchment due to displacement across the fault.

5.2.3. The Mazla Site

[45] At the site of Mazla, we targeted the well-preserved surface F3 and F5 (Figure 5) for dating. These surfaces are flat, dark, paved by pebbles and cobbles (Figure 7). At each site, three well-rooted cobbles of various lithologies (Table 1) and an amalgamated sample of rounded quartz pebbles were collected. The ages are given in Table 1 and Figure 10.

[46] On surface F3, we obtained at the southern site three consistent ages of 93 ± 9 ka (sample 25), 104 ± 10 ka (sample 26) and 119 ± 11 ka (sample 27), the oldest age corresponding to the amalgamated sample. Sample 28, a quartzite cobble, yielded a significantly older age of 257 ± 25 ka. To the north, we obtained two pairs of similar ages. The pair 81 ± 8 ka (amalgamated sample 23) and 82 ± 8 ka (sample 24) are in good agreement with the ages obtained further south. The other two ages are significantly younger: 44 ± 4 ka (sample 21) and 51 ± 5 ka (sample 22). The location of the sampling site, close to a major active channel that separates surface F3 from the younger surface F2 (Figure 5), suggests that the youngest samples may reflect occasional postabandonment contamination of F3, possibly during the deposition of F2. Although data are scarce, this hypothesis is supported by the agreement between the age derived from the amalgamated sample 23 and the age of individual cobbles from the two sampling sites on F3. Based on samples 23 to 27 we calculated an average age of 96 ± 16 ka for F3. The difference in age between the amalgamated samples 27, collected in the southern part, and 23, collected in the northern part, may suggest northward migration of the water flow with time.

[47] On the surface F5, three cobbles provided exposure ages of 319 ± 32 ka (sample 30), 328 ± 33 ka (sample 31) and 362 ± 36 ka (sample 32). The age of the amalgamated sample (312 ± 31 ka, sample 29) is consistent with the individual samples. The four ages lead to an average of 330 ± 22 ka for F5. Similarly to the surface F5 at the site of Risha, these ages are very dependent on how we consider erosion and they should be considered with care.

6. Discussion: Alluvial Fans as a Climatic Record and Their Implications for Late Pleistocene Activity of the Wadi Araba Fault

[48] The combination of detailed morphotectonic analyses and dating of surfaces lead to the morphotectonic map of the Wadi Araba presented on Figure 3. This map shows a comprehensive relative chronology for the emplacement of the late Pleistocene alluvial deposits at the scale of the valley. In sections 6.1 and 6.2, we first discuss the synchronism of alluvial fans emplacement and possible correlation with recognized paleoclimatic events. Next, building on such chronology and the fact that many of these surfaces are offset relative to their feeding catchment due to the motion of the WAF, we provide some insights in the late Pleistocene activity of the WAF.

6.1. Synchronism of Alluvial Fan Deposition Within the Wadi Araba

[49] Previous studies conducted in glaciofluvial and fluvial environments [e.g., *Bull*, 1991; *Van der Woerd et al.*, 2002; *Sharp et al.*, 2003; *Daëron et al.*, 2004; *Mériaux et al.*, 2005; *Regard et al.*, 2006] have shown a close relationship between paleoclimates and the emplacement of alluvial deposits. The relationship between bed load transport, precipitation, and temperature is however not straightforward, especially under arid climatic conditions. In a simplistic picture, higher rainfall would enhance denudation and bed load transport and thus favor deposition of clasts downstream. Yet, other factors such as the vegetation cover and the rainfall regime also influence the efficiency of denudation in the catchment [*Bull*, 1991]. Here, we test the possible climatic control on the deposition of alluvial fans in the Wadi Araba and if any correlation can be established between the phases of alluvium aggradation and any regional or local documented climatic events.

[50] Figure 8 compares the alluvial sequences observed at the sites of Risha, al-Dhawi, and Mazla. At Risha and Mazla, [10]Be CRN dating yielded comparable average exposure age for F5, respectively of 316 ± 24 ka and 330 ± 22 ka. Even if some erosion should be accounted for, the two sites would likely be affected the same way, considering their proximity. Combining the ages from both sites yields a mean age of 324 ± 22 ka for this event of alluvium deposition. All sites exhibit a cluster of ages from ~70 ka to ~130 ka from the deposits F3. At Risha and al-Dhawi, the deposit F3 appears to be divided into 3 sublevels, F3a to F3c, probably due to uplift of the Jabal al-Risha, that favors an earlier abandonment of the alluvial surfaces. F3a was observed at the northern tip of the Jabal al-Risha and dated at 130 ± 19 ka from the al-Dhawi deposit. Surfaces F3b were emplaced at the mouth of Wadi al-Dhawi (108 ± 4 ka), east of the fault, and near the apex of F3c (101 ± 10 ka). The apex of F3c was dated at 71 ± 6 ka. Given the overlap of the [10]Be CRN ages, we consider all the F3 deposits as part of a single alluvial event dated at 102 ± 26 ka. It is worth noticing that both at

Risha and Mazla younger samples of consistent age, at ~50 ka (samples 1, 21 and 22), can be found on F3. Although these cobbles could be part of a more complicated history of burial, remobilization and exposure, they might alternatively reflect a more recent phase of emplacement of alluvial deposits, which would have occurred around 48 ± 5 ka. The alluvial level F4 was only dated at Risha, at 163 ± 19 ka.

[51] Eventually, we have identified three and possibly four episodes of emplacement of alluvial surfaces: 324 ± 22 ka, 163 ± 19 ka, 102 ± 26 ka and more hypothetically 48 ± 5 ka (Figure 8). The synchronous clusters at 324 ± 22 ka and 102 ± 26 ka strongly suggest a uniform response of the bed load transport and stream power of the drainages to some external climatic forcing, at least at the scale of the central Wadi Araba. Previous studies investigated late Quaternary deposits in the Wadi Araba (Figure 3), using ^{10}Be CRN ages [*Klinger et al.*, 2000a, 2003; *Le Béon et al.*, 2010] and OSL dating [*Porat et al.*, 2010]. In spite of some significant dispersion of the ^{10}Be CRN ages, similarly to our results, these three studies show prominent alluvial surfaces that correlate with the 102 ± 26 ka phase of deposition. Such observations and the new ages presented here, all tend to confirm the similarity of response of the local drainages to climatic variations at the scale of the Wadi Araba. It is worth highlighting the lack of fans between 324 ± 22 ka and 163 ± 19 ka, although we cannot rule out a bias due to our sampling strategy that focus on levels that are offset by the fault.

[52] Correlating the three main phases of alluviation that we observed with local and regional documented paleoclimatic records is not straightforward, particularly because the uncertainty on ages is often larger than, or in the order of the frequency of the climatic variations. However, the deposition phase observed around 102 ± 26 ka throughout the Wadi Araba clearly coincides with the interglacial Marine Isotope Stage 5 (MIS-5) [*Emiliani*, 1955; *Shackleton*, 1969], identified as a wetter period both locally and regionally. Several local studies on the Jordanian Plateau, in the Wadi Araba, and in the Negev, mention the occurrence of lake deposits and travertine during MIS-5 [*Schwarcz et al.*, 1979; *Livnat and Kronfeld*, 1985; *Abed et al.*, 2000]. This wet period is also reported regionally from the speleothems of Israeli caves [*Bar-Matthews et al.*, 2003], the pollens and the sapropel layers (organic-rich layers resulting from heavy discharge from the Nile River) observed in marine cores from the Eastern Mediterranean [*Cheddadi and Rossignol-Strick*, 1995; *Rossignol-Strick and Paterne*, 1999]. The depositional event at 163 ± 19 ka occurred during the glacial period MIS-6. It may correlate with a minimum of $\delta^{18}O$ and a high water stand recorded at 150–155 ka in the Israeli caves and with the sapropel 6. Similarly to the 102 ± 26 ka event, it would as well coincide with a noticeably wet period. The oldest phase of alluviation, at 324 ± 22 ka, would correspond to the major interglacial MIS-9. Few local records exist to document whether MIS-9 was a wet or dry period. In addition, this latest correlation should be interpreted carefully as these ages are very sensitive to possible erosion of the surfaces. The lack of fans between ~324 ka and ~163 ka might be explained by the prominence of the 163 ± 19 ka and 102 ± 26 ka wetter periods compared to local climate during the former time period.

6.2. Associating a Feeding Catchment to the Large Abandoned Alluvial Surfaces

[53] To further understand the processes controlling the emplacement of the large abandoned alluvial surfaces described in sections 2–5, we need to associate to each of them a feeding source among the potential large catchments identified in section 3 (Figure 3). Given the ^{10}Be CRN model ages that are as young as late Pleistocene and the wide range of fault slip rates published in the literature (3 mm/yr to 11 mm/yr) (see *Le Béon et al.* [2010] for a complete review), the maximum expected offsets are in the order of ~1 km to ~3.2 km for respectively ~100 ka old and ~320 ka old surfaces, suggesting a fairly close source for those deposits. Hence, the Wadi Musa and the Wadi Huwar are the only possible sources for the Mazla fans and the Risha fans, respectively. The outlets of the other catchments are too far north from the deposits to be reasonably considered.

[54] Attributing a source to the undated alluvial surfaces of Fuhud and Masqara is not straightforward. The closest large catchment that may produce such large alluvial deposits is the Wadi Fidan (Figure 3). Any catchment north of Wadi Fidan can hardly be considered as a potential source for those deposits, as they would have been eroded away when moved in front of the wadi. Several morphologic criteria, however, lead us to discard the Wadi Fidan as a possible feeder. First, if the Wadi Fidan was the source of these deposits, the surfaces should appear to be younger northward. Also, more recent alluvial surfaces are lacking between Masqara and the present-day alluvial fan emplaced by the Wadi Fidan. Second, because the outlet of the Wadi Fidan is located only ~1 km east of the active trace of the WAF, the alluvial fan deposited at its mouth on the western block should exhibit a characteristic fan shape with radial topographic contour lines (Figure 3), unlike the Fuhud and Masqara surfaces, which morphology suggests a rather distal source (section 4.3). Finally, the elevation of the eastern edge of these surfaces is ~150 m higher than the present-day apex of the Wadi Fidan alluvial fan.

[55] Instead, we suggest that the surfaces of Fuhud and Masqara originate from the smaller catchments (up to ~70 km^2) located between the Wadi Fidan and the Wadi Musa. Between these two wadis, in the al-Hiqna Plain, east of the fault, a large bajada forms at the toe of the valley escarpment (Figures 3 and 6). The fairly straight N15°E oriented topographic contour lines of this large bajada, as well as its width, match quite well the morphology of the abandoned deposits of Fuhud and Masqara, suggesting that it is the most probable source for these surfaces.

6.3. Quantifying Cumulative Left-Lateral Offsets and Fault Slip Rates Along the WAF

[56] The morphology of all the abandoned alluvial surfaces described in this study (section 4) shows evidence for late Pleistocene activity on the WAF: the sharp linear eastern edge of the alluvial surfaces and a disturbed drainage network. In addition, both at the sites of Risha and Mazla, we observe a series of deposits that become younger northward, in agreement with a western block moving southward relative to feeding channels located to the east. However, the lack of counterpart across the fault for most surfaces and the smallness of expected offsets (≤1 km to ≤ 3.2 km) relative to

Table 2. Summary of the Offsets and Fault Slip Rates Determined at the Different Sites Investigated in This Study[a]

Surface	Risha/al-Dhawi	Mazla	Fuhud-Masqara
F7	-	2.9–12.8 km; **5430–5930 m** *780–1190* ka	**4950–6150 m** *710–1230* ka
F6	-	1.8–11.5 km; **3600–4440 m**	
F6 riser N	-	**2590–3770 m** *510–880 ka*	-
F5	0.4–8.6 km; **1570–3930 m** 316 ± 24 ka *4.6–13.5 mm/a*	0.4–9.4 km; **1950–4150 m** 330 ± 22 ka *5.5–13.5 mm/a*	-
F4[b]	-	0–8.4 km; **1290–3530 m** 163 ± 19 ka* *7.1–24.5 mm/a*	
F3	-	0–4.8 km; **0–1740 m** 96 ± 16 ka *0–21.8 mm/a*	-
F3a	**930–1350 m** 130 ± 19 ka *6.2–12.2 mm/yr*	-	-
F3c	0–4.0 km; **80–940 m (440 ± 10 m)** 71 ± 6 ka *1.0–14.5 mm/yr (5.5–6.9 mm/yr)*	-	-
F2	-	0–3.4 km; **0–1725 m** 48 ± 5 ka? *0–40.1 mm/a*	-

[a]First values indicate conservative offset ranges, determined from the widest angle that the feeding channel could sweep. Bold values indicate best offsets determined from surface morphology; uncertainties on such offsets may be underestimated. Italic values indicate the fault slip rates derived from the age-offset combination or, for the undated surfaces F6 and F7, the age estimate inferred from the offset and assuming a fault slip rate of 5–7 mm/yr.
[b]Dated only at Risha.

the size of the geomorphic features (~15 km) have made it more difficult to accurately determine the offset associated to each surface. In a first step, we provide here a minimum and a maximum offset for each surface (Table 2) by moving the abandoned surfaces back to the areas where they could have reasonably formed, based on the surface/feeder match proposed in section 6.2. Such offsets range between zero and several kilometers. However, any offset value within these intervals does not necessarily lead to a match of the alluvial surfaces across the fault that is consistent with their morphology. Next, considering the morphology of the surfaces on both sides of the fault, we try to refine the tectonic restoration of surfaces to their initial geometry, based on tentative piercing lines. Doing so, we also reduce the range of possible offset values. In the following, we present only the few significant reconstructions. All other reconstructions are described by *Le Béon* [2008].

6.3.1. Tectonic Reconstructions at the Site of Risha and Al-Dhawi

[57] At Risha, the narrow incision into the Jabal al-Risha at the apex of fan F3c allowed us to determine the axis of the drainage that fed F3c (green line and dotted lines on Figure 9). The axis bisects the angle defined by the risers on both sides of the apex and it is perpendicular to the topographic contour lines downstream the apex. We considered an uncertainty of 5°. Similarly, we determined the axis and solid angle for the water flowing out of the Wadi Huwar based on the geometry of the narrow river channel in the bedrock at the catchment outlet (blue dotted lines on Figure 9). Water probably flew sideways during intermittent periods of time. However, we propose that the most efficient path for the feeding drainage to maintain stream power in order to compete with the uplift of the ridge was to flow straight out of the Wadi Huwar. Hence, we first matched the axis of the fan apex of F3c (green line) with the wadi axis (blue line) to obtain a best offset of

440 ± 10 m. A more conservative range of possible offsets of 80 m to 940 m was derived when matching the solid angles of the wadi and of the fan.

[58] Similar reconstruction for the surface F5 leads to an offset of 1570 m to 3930 m relative to the Wadi Huwar. Because the apex of F5 is not as well defined as on F3c, it leads to larger uncertainty in the reconstruction.

[59] In addition to these two main surfaces, we also considered the dark reddish surface visible at the northern tip of the Jabal al-Risha and which counterpart was identified at the mouth of the Wadi al-Dhawi, east of the WAF (Figure 4). We use the southern edge of the surfaces on both sides of the WAF as a piercing line to tentatively reconstruct the surface. This reconstruction assumes that the active fan east of the fault remained at the same location between ~130 ka (age of the western surface) and ~108 ka (age of the eastern one). East of the fault, the southern riser of the fan follows the contact with an older Pleistocene alluvium (Figure 4). West of the fault, the southern extent of the fan is not clear near the fault trace, but it could be mapped fairly accurately further west. Some uncertainty remains in the reconstruction, as the piercing lines do not extend to the active fault trace. We propose a minimum offset of 930 m (Figure 10a) when extending the southern riser of the eastern surface in the direction of the steepest slope of the eastern surface. Extending westward the southern riser of the eastern surface provides a maximum offset of 1320 m (Figure 10b).

6.3.2. Tectonic Reconstructions at the Site of Mazla

[60] The topographic contour lines and the orientation of the channels incised in the surfaces at Mazla, west of the WAF, indicate the orientation of the steepest slope and therefore the orientation of the water flow that emplaced the surfaces. As noted in section 4.2, this orientation gradually changes from the southern part to northern part of the site. It
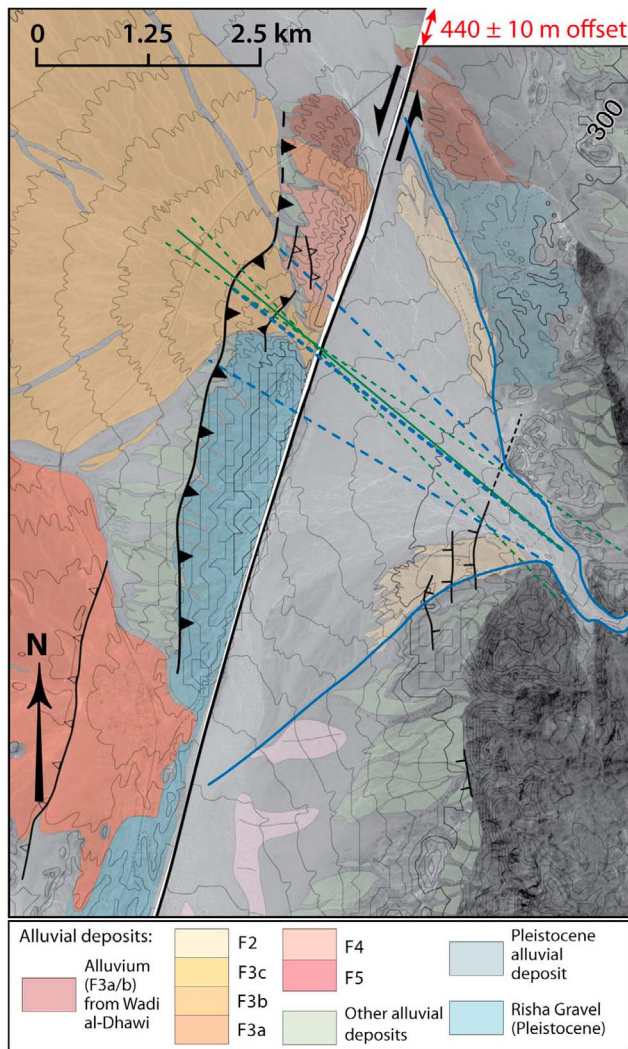
Figure 9. Tectonic reconstruction for the fan F3c at the site of Risha. We matched the axis of the drainage that fed the fan F3c (green lines) with the channel axis (blue dashed lines). We show here the best offset reconstruction of 450 m, the whole offset range being 80–940 m.

suggests that the southern surfaces F7 to F5 were emplaced by a wadi flowing mostly westward, coming out straight from the mouth of the Wadi Musa, while the northern surfaces F3 and F2 were deposited by a wadi flowing rather northwestward. The reconstructions proposed hereafter are built on the assumption that one could adjust the paleowater flow, derived from the contour lines, to the surface of the fan emplaced at the mouth of the Wadi Musa east of the WAF.

[61] We only show here such reconstruction for the surface F3, but similar reconstruction can be done for other surfaces. The topographic contour lines of F3 are well preserved and they can be fitted by subparallel straight lines (white dotted lines on Figure 11), allowing for an accurate determination of the orientation of the water flow that emplaced F3: N42°W ± 2° (red arrows). The orientation of the rills incised in the surface varies between N52°W to the south and N42°W to the north, in relatively good agreement with the topography.

[62] We then need to investigate the position of the fan apex east of the fault. As described in section 4.2, east of the WAF the morphology of the fan surface has changed over time: the active fan is currently located directly west of the outlet of the Wadi Musa, while an older fan mapped as F1/F2 attests to an earlier northwestward influx of clasts (Figures 5 and 11). To the first order, the shape of the topographic contour lines will reflect the distance to the source of the sediments; straight lines will indicate a remote source, while a closer source will imply curvier contour lines. The straight topographic contour lines of F3 require a
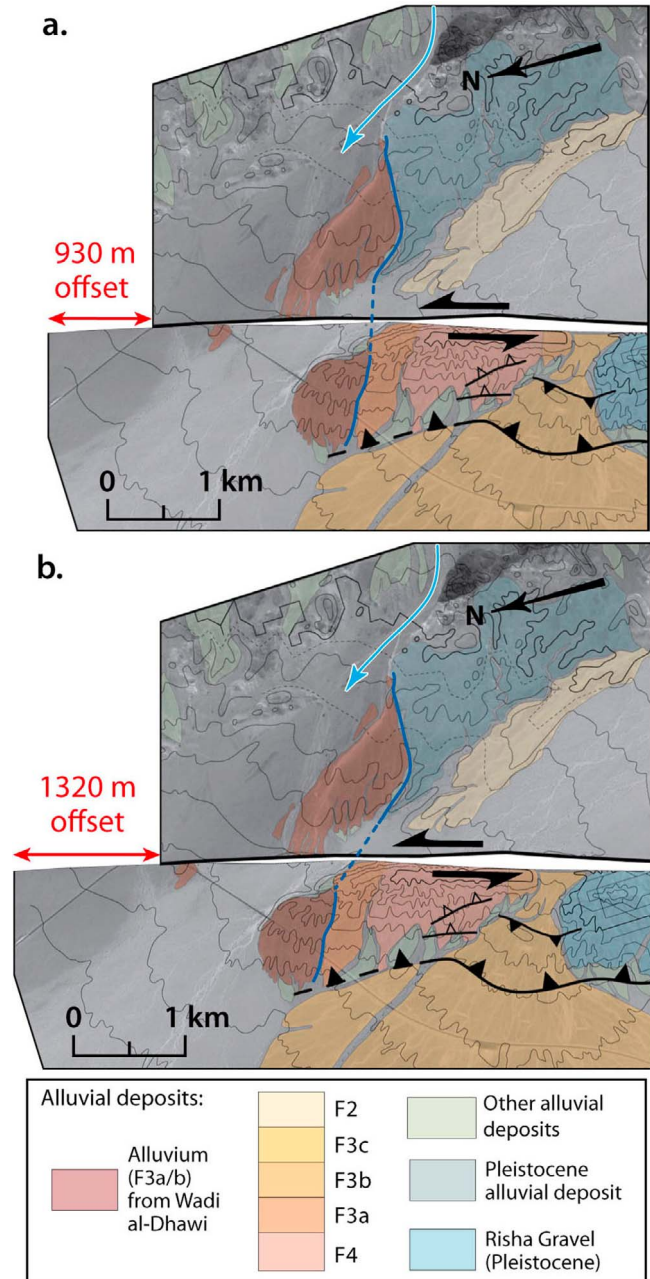

Figure 10. Tectonic reconstructions of the Wadi al-Dhawi fan. (a) Minimum offset of 930 m. (b) Maximum offset of 1320 m. The blue line indicates the southern extent of the surface that we use as piercing line.
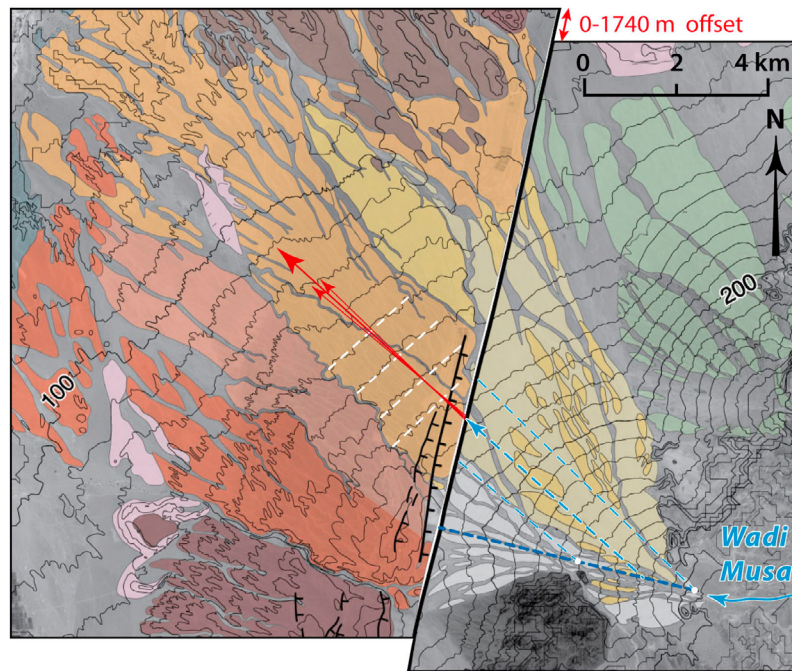
Figure 11. Tectonic reconstruction of the fan F3 at Mazla, offset by 0–1740 m. The offset shown here is 735 m. Red arrows indicate the orientation of the water flow that emplaced F3, determined from the geometry of the topographic contour lines. The white dots bracket the range of possible positions for the fan apex, along the channel axis materialized by the dark blue dashed line. The offset interval is obtained by adjusting the water flow arrows in between the possible apex positions (white dots), as shown by the light blue dashed lines and arrow.

remote source. The fan F1/F2 east of the fault shows that the transition from radial to straight topographic contour lines occurs ~4 km downstream the mouth of Wadi Musa. Thus, the fan apex could be located anywhere between the outlet of the Wadi Musa and the point located 4 km upstream the eastern edge of F3 (extreme positions are indicated by white dots on Figure 11). We placed at these two extreme locations a light blue dashed arrow representative of the axis of the water flow that emplaced F3, which is oriented N42°W. The position of F3 when it was abandoned is obtained by adjusting the water flow arrows to the range of possible positions of the apex in between the light blue dotted lines. We obtain an offset of 0 to 1740 m. Despite well-defined morphology of the surface, the uncertainty on the offset remains high due to the uncertainty on the position of the apex and the oblique angle of the water flow relative to the channel main axis.

[63] Based on a similar reasoning, we propose reconstructions for each surface observed at the site of Mazla. We obtained offsets of 5680 ± 250 m from the channel incised into F7, 4020 ± 420 m for F6, 3180 ± 590 m from the riser between F6 and F5, 3050 ± 1100 m for F5, 2410 ± 1120 m for F4, and 0–1640 m for F2 (Table 2 and Figure 13). The uncertainties remain large, yet the offsets consistently decrease with the relative and absolute ages of the surfaces, giving some confidence in these estimates. Uncertainties increase with decreasing offsets because the water flow that emplaced younger surfaces departs more from the channel axis than for older surfaces.

6.3.3. Tectonic Reconstruction at the Site of Fuhud and Masqara

[64] This reconstruction is based on the difference in morphology between the Masqara and Abu Dubana deposits that suggest a different source for both alluviums. The catchments upstream the al-Hiqna Plain were proposed as the source of the Fuhud and Masqara surfaces. The orientation of topographic contour lines and the elevation of the small surface of Abu Dubana (Figure 6) look similar to the bajada located just north of it, at the toe of the Jabal Hamrat Fidan granitic ridge. Hence, it strongly suggests that the Abu Dubana surface was probably deposited downstream the Jabal Hamrat Fidan. In parallel, the northwestward orientation of the slope on the northern part of the Masqara surface and the northward decrease in elevation of its eastern edge could be explained as a transitional zone from the high bajada of the al-Hiqna Plain, to the east, to the lower Wadi Araba valley floor, to the northwest. Hence, the reconstruction consists in adjusting the contact between the Masqara and Abu Dubana surfaces (white dashed line on Figure 12) in front of the southern tip of the Jabal Hamrat Fidan ridge. It assumes that both alluviums were deposited at the same time period. The position of the contact between the two surfaces at the fault trace is uncertain due to the erosion and deposition of more recent deposits along an active wadi. East of the fault, we assume that the water flow (red dashed arrows) could be running perpendicular to the topographic contour lines or obliquely toward the northwest, similar to the water flow that deposited the Masqara alluvium. We then obtained an offset of 5550 ± 600 m. This reconstruction also aligns the abandoned gully that separates Masqara from Fuhud
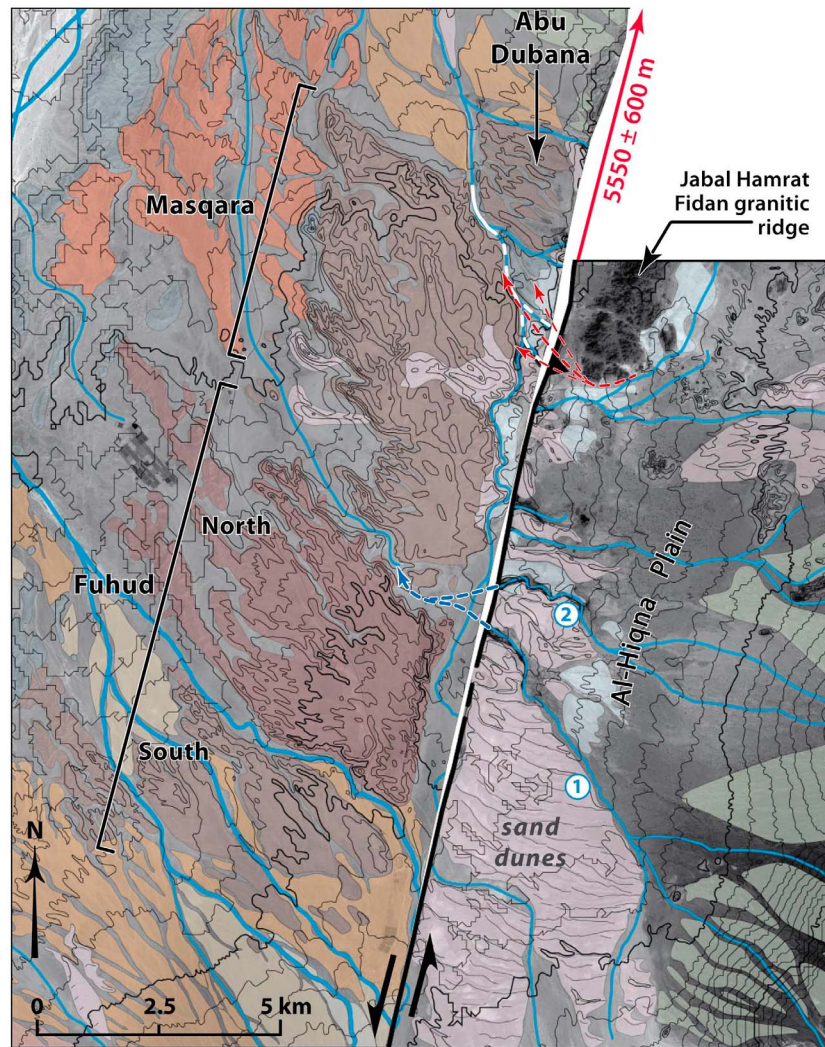
Figure 12. Tectonic reconstruction for the Fuhud, Masqara, and Abu Dubana surfaces. White dashed lines indicate the contact between Abu Dubana and Masqara. Red arrows indicate the possible orientations of the water flow coming down the bajada, around the granitic ridge. As shown by the blue dashed lines, the reconstruction also aligns one or two channels (labeled 1 and 2) to the east of the fault with an abandoned major gully to the west.

with possibly two connecting drainages that originate from the east. The path of these drainages, however, may have changed in the past, as the sand dunes field is likely to have been emplaced after the Masqara surface. Yet, the abandoned drainage is facing the outlet of the largest catchment (70 km²) upstream the bajada (feeding drainage 2 on Figure 12).

6.3.4. Constraints on the Late Pleistocene Slip Rate of the Wadi Araba Fault

[65] The offsets determined at each site and for each morphostratigraphic level are summarized in Table 2 and Figure 13. As mentioned earlier, the offsets presented in the above sections have large uncertainties attached to them, which make them difficult to interpret individually. However, when considered together, a consistent picture emerges: first, at all sites the offsets gradually decrease with surface age, and second, the offset recorded by surfaces of similar age, but located at different sites, are consistent.
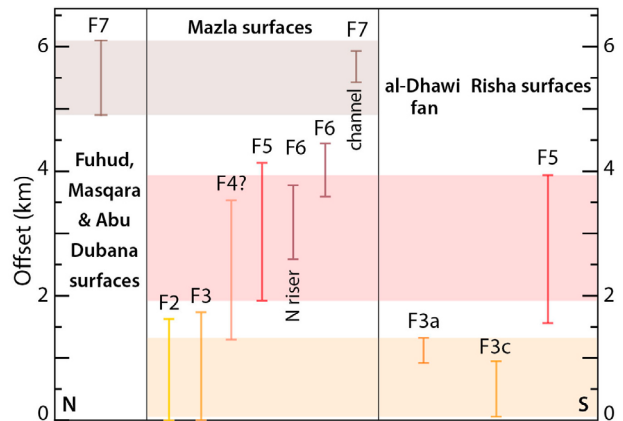

Figure 13. Summary of the best offsets proposed in this study. See also Table 2. Colored rectangles indicate the overlap of offset data at different sites, for F7, F5 and F3.
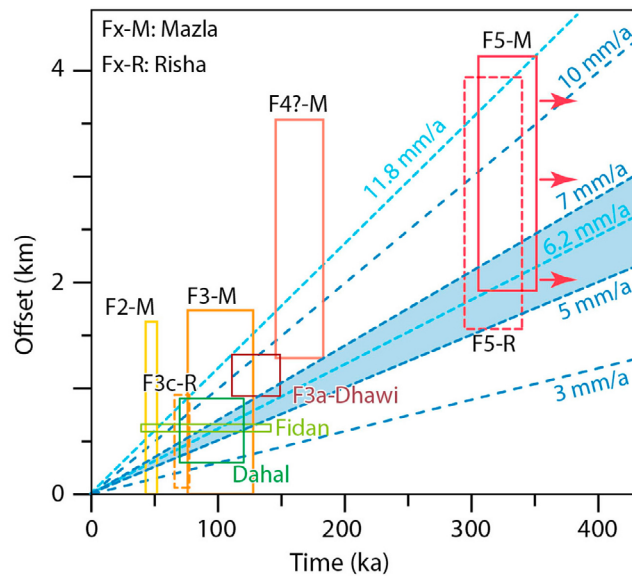
Figure 14. Synthesis of the age and offset data from this study and from previous late Pleistocene studies of *Klinger et al.* [2000a] and *Le Béon et al.* [2010] (Dahal and Fidan green rectangles, respectively). For reference, slip rate trends for 3, 5, 7, and 10 mm/yr are shown, the range 3–7 mm/yr corresponding to the geological fault slip rates. We also plot the narrowest slip rate range of 6.2–11.8 mm/yr determined from the al-Dhawi fan F3a. The data synthesized here, taken together with the geological slip rates, tend to favor slip rate values of 5–7 mm/yr. The question mark associated to the surface F4 at Mazla reminds that the surface itself was not dated. Red arrows indicate that the ages of the surfaces F5 are minimum ages, possibly underestimated in case of erosion.

Hence, such consistency between offsets determined independently supports the relevance of the proposed reconstructions and the overall geomorphic interpretation.

[66] The combination of offsets and ages leads to the individual fault slip rates reported in Table 2 and synthesized on Figure 14. We discuss here only the ranges of fault slip rate that are constrained enough to bring interesting insight on the activity of the fault at the timescale of a few 100 ka. The fault slip rate derived from the fan F3c at Risha is 1.0–14.5 mm/yr since ~71 ka, with a best interval of 5.5–6.9 mm/yr. The al-Dhawi fan F3a provides a consistent slip rate of 6.2–11.8 mm/yr since ~130 ka. The slip rate obtained from the surface correlated to F4 at Mazla, 7.1–24.5 mm/yr, is significantly faster. The lower values only are consistent with the ranges obtained from the fans F3a and F3c at Risha. This result, however, is not as reliable as others given that this particular surface was not dated. The surfaces F5 provided consistent fault slip rates of 4.6–13.5 mm/yr since ~316 ka at Risha and 5.5–13.5 mm/yr since ~330 ka at Mazla. Because the ages are minimum, these slip rates may be considered as maximum values.

6.4. Discussion and Comparison With Previous Work

[67] Some of the alluvial surfaces at Risha and Mazla were previously studied by *Ginat et al.* [1998], together with the conglomerate (the Edom conglomerate) of a paleoriver that used to flow from the Jordanian Plateau to the Mediterranean Sea across the Negev. Based on lithologic compositions, the authors identified the Wadi Musa and the Wadi Huwar as the potential sources of the Edom conglomerate and they concluded that the offset had to be about 15 km to 30 km. Such offsets are correct under the assumption that the river was flowing straight to the west across what is now the Wadi Araba. Stratigraphic constraints provided a poor age control for the Edom conglomerate, which was estimated to be from middle–late Miocene to early Pleistocene [*Ginat et al.*, 1998]. Ginat et al. eventually favored a Pliocene age of 2–5 Ma, which they similarly assigned to the alluvial fans of Risha and Mazla, associated to an offset of 15 km. Then, they obtained a slip rate of 3–7.5 mm/yr, in agreement with earlier studies.

[68] In such reconstruction, the Wadi Musa and the Wadi Fidan (=Wadi Qunei of *Ginat et al.* [1998]) face the fans of Risha and the fans F3 to F5 at Mazla, respectively. The fans F6 and F7 have not been considered. Several aspects of this reconstruction are not consistent with the alluvial sequence we have established from the [10]Be CRN dates and the geomorphic analyses. First, the fan F5 of Risha and the fan F3 of Mazla would have been deposited at the same time, while F5 of Mazla would be the oldest fan and F3 of Risha the youngest. Second, as discussed by the authors, the Edom conglomerate itself does not allow distinguishing between the Wadi Huwar and the Wadi Musa as potential sources. Thus, both offsets of 15 km and 30 km remain possible. Also, the uncertainty on the offset would be significant due to the absence of marker between the catchments outlet, at the eastern edge of the Wadi Araba, and the Edom conglomerate, at the western edge. Hence, the Edom conglomerate alone does not support such a precise fault slip rate of 3–7.5 mm/yr.

[69] The offsets and ages provided in this study complement the previous studies at the ~100 ka timescale and they bring new data covering a longer timescale of a few 100 ka. At the ~100 ka timescale, the slip rate range of 1.0–14.5 mm/yr obtained from F3c at the site of Risha is a little wider than the conservative values of 2.1–12.9 mm/yr and 4.2–20.1 mm/yr proposed by *Klinger et al.* [2000a] and *Le Béon et al.* [2010], respectively. Yet, the best value of 5.5–6.9 mm/yr that we propose agrees quite well with the best values of 3.6–7.1 mm/yr and 5.2–10.9 mm/yr from these two previous studies. The slip rate of 6.2–11.8 mm/yr obtained from F3a at al-Dhawi at a similar timescale provides a tighter lower bound. Taken together, these results suggest that slip rate values of 5–7 mm/yr are more likely for the last ~100 ka. The results derived from the morphostratigraphic level F5 expand the record of the Pleistocene activity of the WAF to the last ~300 ka. The range of maximum slip rate of ~5–14 mm/yr that we obtain overlaps with the ~100 ka slip rates and provides an interesting lower bound which also makes published long-term rates slower than 5 mm/yr less likely. The ~100 ka most likely slip rate values are consistent with the present-day GPS slip rate (3.5–6.3 mm/yr [*Le Béon et al.*, 2008]), the Holocene slip rate [*Klinger et al.*, 2000a; *Niemi et al.*, 2001; *Le Béon et al.*, 2010], and the post-Miocene geological records that converge to 3–7 mm/yr for the southern Dead Sea fault [*Dubertret*, 1932; *Quennell*, 1959; *Freund et al.*, 1968, 1970; *Bartov*, 1980; *Garfunkel and*

Ben-Avraham, 2001]. The agreement between slip rates spanning different timescales supports a simple scenario of constant-over-time fault kinematics [*Le Béon et al.*, 2010], at least for time periods longer than ~10 ka. Extensive study of the earthquake cycle during the Holocene is still lacking today on the WAF.

[70] Although faster fault slip rates in the range 7–12 mm/yr cannot be excluded during the late Pleistocene, temporal variations in fault slip rate are expected to average out when longer time periods are considered. We may thus consider a long-term fault slip rate of 5–7 mm/yr to propose age estimates for the morphostratigraphic levels F6 and F7 based on their offset. We obtain age estimates of 510–880 ka for F6 and 710–1230 Ma for F7 (Table 2). The gradual evolution in the morphology of the successive alluvial fans at Mazla suggests a limited time interval in between the emplacement of the each fan, and thus favors younger ages, i.e., a faster fault slip rate. Dating of these surfaces should include the analysis of sections into the deposits and of CRN depth profiles in order to identify possible soil processes to be taken into account in the dating strategy and to determine inheritance, exposure ages, and erosion rates [e.g., *Matmon et al.*, 2009; *Hidy et al.*, 2010].

References

Abed, A. M., P. Carbonel, J. Collina-Girard, M. Fontugne, N. Petit-Maire, J.-C. Reyss, and S. Yasin (2000), Un paléolac du dernier interglaciaire pléistocene dans l'extrême-Sud hyperaride de la Jordanie, *C. R. Acad. Sci., Ser. IIA*, 330, 259–264, doi:10.1016/S1251-8050(00)00111-7.

Alchalbi, A., et al. (2010), Crustal deformation in northwestern Arabia from GPS measurements in Syria: Slow slip rate along the northern Dead Sea fault, *Geophys. J. Int.*, 180, 125–135, doi:10.1111/j.1365-1246X.2009.04431.x.

Amit, R., J. B. J. Harrisson, Y. Enzel, and N. Porat (1996), Soils as a tool for estimating ages of Quaternary fault scarps in a hyperarid environment: The southern Arava valley, the Dead Sea Rift, Israel, *Catena*, 28, 21–45, doi:10.1016/S0341-8162(96)00028-8.

Anderson, R. S., J. L. Repka, and G. S. Dick (1996), Explicit treatment of inheritance in dating depositional surfaces using in situ ^{10}Be and ^{26}Al, *Geology*, 24(1), 47–51, doi:10.1130/0091-7613(1996)024<0047:ETOIID>2.3.CO;2.

Balco, G., J. O. Stone, N. A. Lifton, and T. Dunai (2008), A complete and easily accessible means of calculating surface exposure ages or erosion rates from ^{10}Be and ^{26}Al measurements, *Quat. Geochronol.*, 3, 174–195, doi:10.1016/j.quageo.2007.12.001.

Barjous, M. O. (1995), Geological map of Petra and Wadi al-Lahyana, map sheets 3050-I and 3050-IV, scale 1:50,000, Nat. Resour. Auth. of the Hashemite Kingdom of Jordan, Amman.

Barjous, M. O. (2003), The geology of Petra and Wadi Al-Lahyana area, map sheets no. 3050-I and 3050-IV, *Bull. 56*, Nat. Resour. Auth. of the Hashemite Kingdom of Jordan, Amman.

Bar-Matthews, M., A. Ayalon, M. Gilmour, A. Matthews, and C. J. Hawkesworth (2003), Sea-land oxygen isotopic relationships from planktonic foraminifera and speleothems in the eastern Mediterranean region and their implication for paleorainfall during interglacial intervals, *Geochim. Cosmochim. Acta*, 67(17), 3181–3199, doi:10.1016/S0016-7037(02)01031-1.

Bartov, Y. (1994), *Geological photomap of Israel and adjacent areas*, scale 1:750,000, Geol. Surv. of Israel, Jerusalem.

Bartov, Y., G. Steinitz, M. Eyal, and Y. Eyal (1980), Sinistral movement along the Gulf of Aquaba—its age and relation to the opening of the Red Sea, *Nature*, 285, 220–222.

Bartov, Y., M. Stein, Y. Enzel, A. Agnon, and Z. Reches (2002), Lake levels and sequence stratigraphy of Lake Lisan, the late Pleistocene precursor of the Dead Sea, *Quat. Res.*, 57, 9–21, doi:10.1006/qres.2001.2284.

Bender, F. (1974), Explanatory notes on the geological map of the Wadi Araba, Jordan, scale 1:100,000, *Geol. Jahrb., Reihe B*, 10, 62 pp.

Bender, F., G. van den Boom, R. Busse, W. Heimbach, K. Khdeir, M. Lahloub, W. Lillich, and G. Wiesemann (1968), *Geological map of Jordan*, scale 1:250,000, sheet Aqaba-Ma'an, Geol. Surv., Hannover, Germany.

Bull, W. B. (1962), Relations of alluvial fan size and slope to drainage basin size and lithology in western Fresno County, California, *U.S. Geol. Surv. Prof. Pap.*, 450-B, 51–53.

Bull, W. B. (1991), *Geomorphic Responses to Climatic Change*, Oxford Univ. Press, New York.

Cheddadi, R., and M. Rossignol-Strick (1995), Eastern Mediterranean quaternary paleoclimate from pollen and isotope records of marine cores in the Nile cone area, *Paleoceanography*, 10, 291–300, doi:10.1029/94PA02672.

Courtillot, V., R. Armijo, and P. Tapponnier (1987), The Sinai triple junction revisited, *Tectonophysics*, 141, 181–190, doi:10.1016/0040-1951(87)90184-3.

Daëron, M., L. Benedetti, P. Tapponnier, A. Sursock, and R. Finkel (2004), Constraints on the post ~25-ka slip rate of the Yammouneh fault (Lebanon) using in-situ cosmogenic Cl^{36} dating of offset limestone-clast fans, *Earth Planet. Sci. Lett.*, 227, 105–119, doi:10.1016/j.epsl.2004.07.014.

Dubertret, L. (1932), Les formes structurales de la Syrie et de la Palestine, *C. R. Acad. Sci.*, 195, 65–67.

Elias, A., et al. (2007), Active thrusting offshore Mount Lebanon: Source of the tsunamigenic A.D. 551 Beirut-Tripoli earthquake, *Geology*, 35, 755–758, doi:10.1130/G2363A.

Emiliani, C. (1955), Pleistocene temperatures, *J. Geol.*, 63(6), 538–578, doi:10.1086/626295.

Ferry, M., M. Meghraoui, N. Abou Karaki, M. Al-Taj, H. Amoush, S. Al-Dhaisat, and M. Barjous (2007), A 48-kyr-long slip rate history for the Jordan Valley segment of the Dead Sea fault, *Earth Planet. Sci. Lett.*, 260, 394–406, doi:10.1016/j.epsl.2007.05.049.

Ferry, M., M. Meghraoui, N. Abou Karaki, M. Al-Taj, and L. Khalil (2011), Episodic behavior of the Jordan Valley section of the Dead Sea fault inferred from a 14-ka-long integrated catalog of large earthquakes, *Bull. Seismol. Soc. Am.*, 101, 39–67, doi:10.1785/0120100097.

Freund, R., I. Zak, and Z. Garfunkel (1968), Age and rate of the sinistral movement along the Dead Sea Rift, *Nature*, 220, 253–255, doi:10.1038/220253a0.

Freund, R., Z. Garfunkel, I. Zak, M. Goldberg, T. Weisbrod, and B. Derin (1970), The shear along the Dead Sea rift, *Philos. Trans. R. Soc. London, Ser. A*, 267, 107–130, doi:10.1098/rsta.1970.0027.

Frumkin, A. (1997), The Holocene history of the Dead Sea lake levels, in *The Dead Sea: The Lake and Its Setting*, edited by T. M. Niemi et al., pp. 237–248, Oxford Univ. Press, New York.

Garfunkel, Z. (1981), Internal structure of the Dead Sea leaky transform (rift) in relation to plate kinematics, *Tectonophysics*, 80, 81–108, doi:10.1016/0040-1951(81)90143-8.

Garfunkel, Z., and Z. Ben-Avraham (2001), Basins along the Dead Sea Transform, in *Peri-Tethys Memoir*, vol. 6, *Peri-Tethyan Rift/Wrench Basins and Passive Margins*, edited by W. C. P. A. Ziegler, et al., pp. 607–627, Mem. Mus. Natl. Hist. Nat., Paris.

Garfunkel, Z., and A. Horowitz (1966), The upper Tertiary and Qauternary morphology of the Negev, Israel, *Isr. J. Earth Sci.*, 15, 101–117.

Garfunkel, Z., I. Zak, and R. Freund (1981), Active faulting in the Dead Sea Rift, *Tectonophysics*, 80, 1–26, doi:10.1016/0040-1951(81)90139-6.

Ginat, H., Y. Enzel, and Y. Avni (1998), Translocated Plio-Pleistocene drainage systems along the Arava fault of the Dead Sea Transform, *Tectonophysics*, 284, 151–160.

Gosse, J. C., and F. M. Phillips (2001), Terrestrial in situ cosmogenic nuclides: Theory and application, *Quat. Sci. Rev.*, 20, 1475–1560, doi:10.1016/S0277-3791(00)00171-2.

Greenbaum, N., A. Ben-Zvi, I. Haviv, and Y. Enzel (2006), The hydrology and paleohydrology of the Dead Sea tributaries, *Spec. Pap. Geol. Soc. Am.*, 401, 63–93.

Guralnik, B., A. Matmon, Y. Avni, and D. Fink (2010), ^{10}Be exposure ages of ancient desert pavements reveal Quaternary evolution of the Dead Sea drainage basin and rift margin tilting, *Earth Planet. Sci. Lett.*, 290, 132–141, doi:10.1016/j.epsl.2009.12.012.

Harvey, A. M. (1997), The role of alluvial fans in arid zone fluvial systems, in *Arid Zone Geomorphology: Process, Form and Change in Drylands*, 2nd ed., edited by D. S. G. Thomas, pp. 231–259, John Wiley, Chichester, U. K.

Hatcher, R. D., I. Zietz, R. D. Regan, and M. Abu-Ajamieh (1981), Sinistral strike-slip motion on the Dead Sea Rift: Confirmation from new magnetic data, *Geology*, 9, 458–462, doi:10.1130/0091-7613(1981)9<458:SSMOTD>2.0.CO;2.

Hetzel, R., S. Niedermann, M. Tao, P. W. Kubik, S. Ivy-Ochs, B. Gao, and M. R. Strecker (2002), Low slip rates and long-term preservation of geomorphic features in Central Asia, *Nature*, *417*, 428–432, doi:10.1038/417428a.

Hidy, A. J., J. C. Gosse, J. L. Pederson, J. P. Mattern, and R. C. Finkel (2010), A geologically constrained Monte Carlo approach to modeling exposure ages from profiles of cosmogenic nuclides: An example from Lees Ferry, Arizona, *Geochem. Geophys. Geosyst.*, *11*, Q0AA10, doi:10.1029/2010GC003084.

Ibrahim, K. M. (1990), Geological map of Wadi Gharandal, sheet 3050 III, scale 1:50,000, Nat. Resour. Auth. of the Hashemite Kingdom of Jordan, Amman.

Kaufman, A., Y. Yechieli, and M. Gardosh (1992), Reevaluation of the lake-sediment chronology in the Dead Sea basin, Israel, based on new ^{230}Th/U dates, *Quat. Res.*, *38*, 292–304, doi:10.1016/0033-5894(92)90039-L.

Klinger, Y., J. P. Avouac, N. Abou Karaki, L. Dorbath, D. Bourles, and J. L. Reyss (2000a), Slip rate on the Dead Sea transform fault in northern Araba Valley (Jordan), *Geophys. J. Int.*, *142*, 755–768, doi:10.1046/j.1365-246x.2000.00165.x.

Klinger, Y., J. P. Avouac, L. Dorbath, N. Abou Karaki, and N. Tisnerat (2000b), Seismic behaviour of the Dead Sea fault along Araba Valley, Jordan, *Geophys. J. Int.*, *142*, 769–782, doi:10.1046/j.1365-246x.2000.00166.x.

Klinger, Y., J.-P. Avouac, D. Bourles, and N. Tisnerat (2003), Alluvial deposition and lake-level fluctuations forced by late Quaternary climate change: The Dead Sea case example, *Sediment. Geol.*, *162*, 119–139, doi:10.1016/j.sedgeo.2003.07.001.

Kohl, C. P., and K. Nishiizumi (1992), Chemical isolation of quartz for measurement of in situ-produced cosmogenic nuclides, *Geochim. Cosmochim. Acta*, *56*, 3583–3587.

Lal, D. (1991), Cosmic ray labeling of erosion surfaces: In situ production rates and erosion models, *Earth Planet. Sci. Lett.*, *104*, 424–439, doi:10.1016/0012-821X(91)90220-C.

Le Béon, M. (2008), Cinématique d'un segment de faille décrochante à différentes échelles de temps: La faille du Wadi Araba, segment sud de la faille transformante du Levant [in English], PhD thesis, 304 pp., Inst. de Phys. du Globe, Paris.

Le Béon, M., Y. Klinger, A.-Q. Amrat, A. Agnon, L. Dorbath, G. Baer, J.-C. Ruegg, O. Charade, and O. Mayyas (2008), Slip rate and locking-depth from GPS profiles across the southern Dead Sea Transform, *J. Geophys. Res.*, *113*, B11403, doi:10.1029/2007JB005280.

Le Béon, M., Y. Klinger, M. Al-Qaryouti, A.-S. Mériaux, R. C. Finkel, A. Elias, O. Mayyas, F. J. Ryerson, and P. Tapponnier (2010), Early Holocene and late Pleistocene slip rate of the southern Dead Sea fault determined from ^{10}Be cosmogenic dating of offset alluvial deposits, *J. Geophys. Res.*, *115*, B11414, doi:10.1029/2009JB007198.

Livnat, A., and J. Kronfeld (1985), Paleoclimatic implications of U-series dates for lake sediments and travertines in the Arava Rift Valley, Israel, *Quat. Res.*, *24*, 164–172, doi:10.1016/0033-5894(85)90003-1.

Makovsky, Y., A. Wunch, R. Areily, Y. Shaked, A. Rivlin, A. Shemesh, Z. Ben Avraham, and A. Agnon (2008), Quaternary transform kinematics constrained by sequence stratigraphy and submerged coastline features: The Gulf of Aqaba, *Earth Planet. Sci. Lett.*, *271*, 109–122, doi:10.1016/j.epsl.2008.1003.1057.

Marco, S., T. K. Rockwell, A. Heimann, U. Frieslander, and A. Agnon (2005), Late Holocene activity of the Dead Sea Transform revealed in 3D palaeoseismic trenches on the Jordan Gorge segment, *Earth Planet. Sci. Lett.*, *234*, 189–205, doi:10.1016/j.epsl.2005.01.017.

Matmon, A., O. Simhai, R. Amit, I. Haviv, N. Porat, E. McDonald, L. Benedetti, and R. Finkel (2009), Desert pavement-coated surfaces in extreme deserts present the longest-lived landforms on Earth, *Geol. Soc. Am. Bull.*, *121*, 688–697, doi:10.1130/B26422.26421.

Mériaux, A.-S., F. J. Ryerson, P. Tapponnier, J. Van der Woerd, R. C. Finkel, X. Xu, Z. Xu, and M. W. Caffee (2004), Rapid slip along the central Altyn Tagh fault: Morphochronologic evidence from Cherchen He and Sulamu Tagh, *J. Geophys. Res.*, *109*, B06401, doi:10.1029/2003JB002558.

Mériaux, A.-S., et al. (2005), The Aksay segment of the northern Altyn Tagh fault: Tectonic geomorphology, landscape evolution, and Holocene slip rate, *J. Geophys. Res.*, *110*, B04404, doi:10.1029/2004JB003210.

Mériaux, A.-S., K. Sieh, R. C. Finkel, C. M. Rubin, M. H. Taylor, A. J. Meltzner, and F. J. Ryerson (2009), Kinematic behavior of southern Alaska constrained by westward decreasing postglacial slip rates on the Denali fault, Alaska, *J. Geophys. Res.*, *114*, B03404, doi:10.1029/2007JB005053.

Niemi, T. M., H. W. Zhang, M. Atallah, and J. B. J. Harrison (2001), late Pleistocene and Holocene slip rate of the northern Wadi Araba fault, Dead Sea Transform, Jordan, *J. Seismol.*, *5*, 449–474, doi:10.1023/A:1011487912054.

Nishiizumi, K., M. Imamura, M. W. Caffee, J. R. Southon, R. C. Finkel, and J. McAninch (2007), Absolute calibration of ^{10}Be AMS standards, *Nucl. Instrum. Methods Phys. Res., Sect. B*, *258*, 403–413, doi:10.1016/j.nimb.2007.01.297.

Porat, N., R. Amit, Y. Enzel, E. Zilberman, Y. Avni, H. Ginat, and D. Gluck (2010), Abandonment ages of alluvial landforms in the hyperarid Negev determined by luminescence, *J. Arid. Environ.*, *74*, 861–869, doi:10.1016/j.jaridenv.2009.1010.1018.

Quade, J. (2001), Desert pavements and associated rock varnish in the Mojave Desert: How old can they be?, *Geology*, *29*(9), 855–858, doi:10.1130/0091-7613(2001)029<0855:DPAARV>2.0.CO;2.

Quennell, A. M. (1958), the structural and geomorphic evolution of the Dead Sea Rift, *Q. J. Geol. Soc. London*, *114*, 1–24, doi:10.1144/gsjgs.114.1.0001.

Quennell, A. (1959), Tectonics of the Dead Sea rift, paper presented at the 20th International Geological Congress, pp. 385–405, Assoc. of African Geol. Serv., Mexico City.

Rabb'a, I. (1991), Geological map of Al-Qurayqira (Jabal Hamra Faddan), sheet 3051 II, scale 1:50,000, Nat. Resour. Auth. of the Hashemite Kingdom of Jordan, Amman.

Rabb'a, I. (1994), The geology of the Al-Qurayqira (Jabal Hamra Faddan) map, sheet 3051 II, Nat. Resour. Auth. of the Hashemite Kingdom of Jordan, Amman.

Regard, V., O. Bellier, R. Braucher, F. Gasse, D. Bourlès, J. Mercier, J.-C. Thomas, M. R. Abbassi, E. Shabanian, and S. Soleymani (2006), ^{10}Be dating of alluvial deposits from southeastern Iran (the Hormoz Strait area), *Palaeogeogr. Palaeoclimatol. Palaeoecol.*, *242*, 36–53, doi:10.1016/j.palaeo.2006.05.012.

Reilinger, R., et al. (2006), GPS constraints on continental deformation in the Africa-Arabia-Eurasia continental collision zone and implications for the dynamics of plate interactions, *J. Geophys. Res.*, *111*, B05411, doi:10.1029/2005JB004051.

Repka, J. L., R. S. Anderson, and R. C. Finkel (1997), Cosmogenic dating of fluvial terraces, Fremont River, Utah, *Earth Planet. Sci. Lett.*, *152*, 59–73, doi:10.1016/S0012-821X(97)00149-0.

Ritz, J.-F., R. Vassallo, R. Braucher, E. T. Brown, S. Carretier, and D. Bourles (2006), Using in situ–produced ^{10}Be to quantify active tectonics in the Gurvan Bogd mountain range (Gobi-Altay, Mongolia), *Spec. Pap. Geol. Soc. Am.*, *415*, 87–110.

Rohais, S. (2007), Architecture stratigraphique et flux sédimentaires sur la marge sud du Golfe de Corinthe (Grèce): Analyse de terrain, modélisations expérimentales et numériques, PhD thesis, 382 pp., Univ. de Rennes I, Rennes, France.

Rossignol-Strick, M., and M. Paterne (1999), A synthetic pollen record of the eastern Mediterranean sapropels of the last 1 Ma: Implications for the time-scale and formation of sapropels, *Mar. Geol.*, *153*, 221–237, doi:10.1016/S0025-3227(98)00080-2.

Ryerson, F. J., P. Tapponnier, R. C. Finkel, A.-S. Meriaux, J. Van der Woerd, C. Lasserre, M.-L. Chevalier, X. Xu, H. Li, and G. C. P. King (2006), Applications of morphochronology to the active tectonics of Tibet, in *In Situ-Produced Cosmogenic Nuclides and Quantification of Geological Processes*, edited by L. L. Siame et al., *Spec. Pap. Geol. Soc. Am.*, *415*, 61–86, doi:10.1130/2006.2415(05).

Schmidt, S., R. Hetzel, J. Kuhlmann, F. Mingorance, and V. A. Ramos (2011), A note of caution on the use of boulders for exposure dating of depositional surfaces, *Earth Planet. Sci. Lett.*, *302*, 60–70, doi:10.1016/j.epsl.2010.11.039.

Schwarcz, H. P., B. Blackwell, P. Goldberg, and A. E. Marks (1979), Uranium series dating of travertine from archeological sites, Nahal Zin, Israel, *Nature*, *277*, 558–560, doi:10.1038/277558a0.

Shackleton, N. J. (1969), The last interglacial in the marine and terrestrial records, *Proc. R. Soc. London, Ser. B*, *174*, 135–154, doi:10.1098/rspb.1969.0085.

Sharp, W. D., K. R. Ludwig, O. A. Chadwick, R. Amundson, and L. L. Glaser (2003), Dating fluvial terraces by ^{230}Th/U on pedogenic carbonate, Wind River Basin, Wyoming, *Quat. Res.*, *59*, 139–150, doi:10.1016/S0033-5894(03)00003-6.

Sneh, A., Y. Bartov, T. Weissbrod, and M. Rosensaft (1998a), Geological map of Israel, scale 1:200,000, sheet 3, Geol. Surv. of Israel, Jerusalem.

Sneh, A., Y. Bartov, T. Weissbrod, and M. Rosensaft (1998b), Geological map of Israel, scale 1:200,000, sheet 4, Geol. Surv. of Israel, Jerusalem.

Sneh, A., Y. Bartov, T. Weissbrod, and M. Rosensaft (2000), Geological shaded-relief map of Israel and environs, scale 1:500,000, Geol. Surv. of Israel, Jerusalem.

Stone, J. O. (2000), Air pressure and cosmogenic isotope production, *J. Geophys. Res.*, *105*, 23,753–23,759, doi:10.1029/2000JB900181.

Tarawneh, B. (1991), Geological map of Fifa, map sheet 3051-I, scale 1:50,000, Nat. Resour. Auth. of the Hashemite Kingdom of Jordan, Amman.

Van der Woerd, J., F. J. Ryerson, P. Tapponnier, Y. Gaudemer, R. Finkel, A. S. Meriaux, M. Caffee, G. Zao, and Q. He (1998), Holocene left slip-rate determined by cosmogenic surface dating on the Xidatan segment of the Kunlun fault (Qinghai, China), *Geology*, *26*, 695–698, doi:10.1130/0091-7613(1998)026<0695:HLSRDB>2.3.CO;2.

Van der Woerd, J., A. S. Meriaux, Y. Klinger, F. J. Ryerson, Y. Gaudemer, and P. Tapponnier (2002), The 14 November 2001, M_w = 7.8 Kokoxili earthquake in northern Tibet (Qinghai Province, China), *Seismol. Res. Lett.*, *73*, 125–135, doi:10.1785/gssrl.73.2.125.

Van der Woerd, J., Y. Klinger, K. Sieh, P. Tapponnier, F. J. Ryerson, and A.-S. Mériaux (2006), Long-term slip rate of the southern San Andreas fault from [10]Be-[26]Al surface exposure dating of an offset alluvial fan, *J. Geophys. Res.*, *111*, B04407, doi:10.1029/2004JB003559.

Waldmann, N., A. Starinsky, and M. Stein (2007), Primary carbonates and Ca-chloride brines as monitors of a paleo-hydrological regime in the Dead Sea basin, *Quat. Sci. Rev.*, *26*, 2219–2228, doi:10.1016/j.quascirev.2007.04.019.

Wdowinski, S., Y. Bock, G. Baer, L. Prawirodirdjo, N. Bechor, S. Naaman, R. Knafo, Y. Forrai, and Y. Melzer (2004), GPS measurements of current crustal movements along the Dead Sea fault, *J. Geophys. Res.*, *109*, B05403, doi:10.1029/2003JB002640.

Wells, S. G., L. D. McFadden, J. Poths, and C. T. Olinger (1995), Cosmogenic [3]He surface-exposure dating of stone pavements: Implications for landscape evolution in deserts, *Geology*, *23*, 613–616, doi:10.1130/0091-7613(1995)023<0613:CHSEDO>2.3.CO;2.